Biointerface Research in Applied Chemistry
Open-Access Journal (ISSN: 2069-5837)

Article
Volume 16, Issue 3, 2026, 83
https://doi.org/10.33263/BRIAC163.083

Necessity of Merging Dual-Action SDHI and Strobilurin Fungicides with Microbial Bio-Fungicides to Counter Genetic Resistance: A Molecular Docking Study

Oktay Bıyıklıoğlu [1], Majid Monajjemi [1,*], Fatemeh Mollaamin [2], Talip Çeter [1]

[1] Department of Biology, Faculty of Science, Kastamonu University, Kastamonu, Turkey
[2] Department of Biomedical Engineering, Faculty of Engineering and Architecture, Kastamonu University, Kastamonu, Turkey
* Correspondence: mmonajjemi@kastamonu.edu.tr;

Received: 26.01.2026; Accepted: 12.05.2026; Published: 15.06.2026

Abstract: The increasing prevalence of fungicide-resistant pathogens, exacerbated by global warming and climate-driven changes in forest ecosystems, poses a major threat to agricultural productivity and food security. To address this challenge, we investigated the design of dual-activated fungicides combining SDHI (succinate dehydrogenase inhibitors) and QoI (strobilurin) pharmacophores, alongside microbial bio-fungicides. Novel hybrid structures were generated by merging SDHI and strobilurin moieties and were evaluated through molecular docking simulations against the active sites of fungal plant pathogens. The results demonstrated that the hybrid compounds exhibited more favorable binding energies (more negative ΔG) compared with several commercial fungicides, indicating enhanced inhibitory potential. In parallel, the aromaticity of central rings in the SDHI and strobilurin fragments was quantified using nucleus-independent chemical shift (NICS) calculations, revealing a linear correlation between ring aromaticity and predicted fungicidal activity. This relationship provides a rational framework for predicting the performance of dual-acting fungicides under varying environmental conditions, including temperature, soil pH, and local climate factors. The findings support the central hypothesis that climate-driven increases in fungal resistance can be mitigated by designing dual-activated fungicides with optimized aromaticity, thereby enhancing binding affinity at fungal targets and improving overall inhibitory activity. This approach enables the rational design of climate-adaptive pesticides for fruits and vegetables, combining synthetic and microbial strategies to maintain efficacy against resistant strains while addressing emerging agricultural challenges.

Keywords: SDHI; QoI; pesticides; fungicides; climate changing; NICS; S-NICS

1. Introduction

The effectiveness of fungicides is diminishing year by year due to climate change, global warming, and the modernization of agricultural practices. Accurate analysis indicates that increasing fungicide resistance, coupled with industrial agriculture, poses serious risks to human health and food security. While fungal resistance arises as a molecular biological phenomenon, human practices, including uncontrolled agricultural technologies, excessive fungicide use, and global trade of crops, livestock, and pests, significantly contribute to its

spread. The expansion of industrial agriculture, unrestricted application of fungicides to maximize yields, and deforestation further amplify the geographical reach of pathogenic fungi. For example, reports from 2014 in Europe highlighted that *Aspergillus*, a fungus capable of causing serious human disease, has developed resistance to azole fungicides widely used in agriculture. Addressing this growing problem requires adopting agroecological farming practices that minimize or eliminate the use of chemical fungicides, pesticides, and antibiotics. Since chemical and pharmaceutical industries develop more potent pesticides, the risk of accelerating genetic mutations in fungi increases, potentially exacerbating public health threats. Additionally, human-induced fires, including the burning of agricultural waste, contribute to soil degradation, air pollution, and damage to water bodies, further threatening ecosystems and human life. In this context, the development and use of dual-action SDHI–strobilurin fungicides, integrated with environmentally conscious practices, represent a promising strategy to maintain crop protection while minimizing ecological and public health impacts.

2. Dangerous Fungi for Fruits

2.1. Fungi for the cherry family.

Cherry leaf spot (CLS), caused by the fungus *Blumeriella jaapii*, is one of the most dangerous diseases on Cherry and sour/tart cherry in the world. Ascospores of *B. jaapii* are created in apothecia at the end of winter through leaves on the orchard floor. These fungus ascospores are generally released from petal fall and infect the plant through the stomata. In the season of blooming and during medium warm and wet climates, the first infections can appear on bract leaves adjacent to flowers; this condition usually causes “CLS epidemics", which are a negative reason for fruit ripening. *Blumeriella jaapii* is a fertile sporulator on ‘Montmorency’, and lumpen conidia, observable, appeared on the axial leaves zone in acervuli (Figure 1). The conidia are readily prevalent in rainy, windy climates, causing secondary infections through the pores, making management of CLS considerably harder under these conditions. Due to the high capability of ‘Montmorency’, CLS controlling is totally dependent upon the use of a broad range of fungicides containing chlorothalonil, captan, and copper [1].

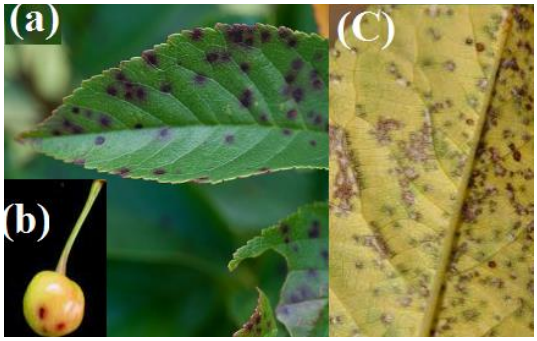

Figure 1. Various cherry leaf spots (CLS). (a): fungus Blumeriella jaapii; (b); lumpen conidia, observable, on the axial leaves zone in acervuli (c): CLS epidemics, which are a negative reason for fruit ripening

Nevertheless, growers have traditionally preferred single-site fungicides that are either systemic or Translocular; therefore, these fungicides can control powdery mildew and brown rot. Resistance to the sterol demethylase inhibitor, fungicide category, appeared in the past decades [2]. This disease was caused by the repeated expression of the CYP51 gene from a promoter insertion containing a portion of the DNA sequence via a transposable element (Figure 2-a) [3]. Tebuconazole is a triazole fungicide used in agriculture to treat CLS-causing

pathogenic fungi. Although the World Food and Drug Administration stated there is no risk to humans from fungicides, the Protection Agency Office of Pesticide Programs carcinogen list lists it as a C, meaning possible carcinogen.

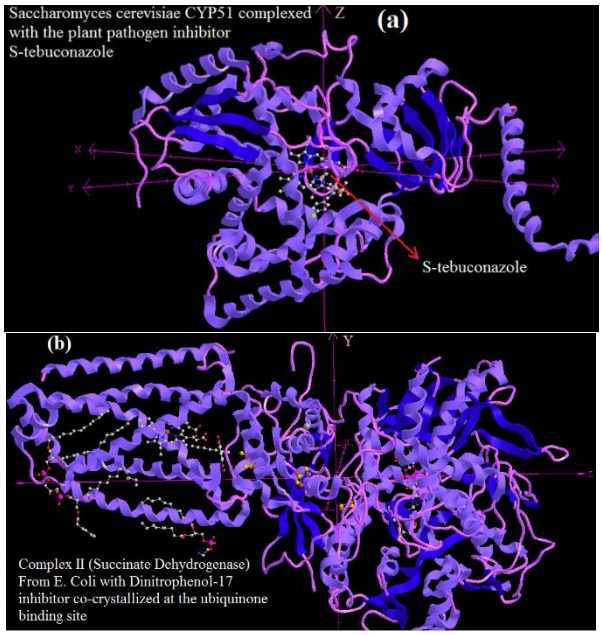

Figure 2. (a) *Saccharomyces cerevisiae* CYP51 complexes with the plant pathogen inhibitor S-tebuconazole; **(b)** Succinate Dehydrogenase from *E. coli.*

Succinate dehydrogenase inhibitors (SDHI) (Figure 2-b) are one of the enzymatic proteins of the tricarboxylic acid cycle from the Krebs cycle, which is able to react to complex II of the mitochondrial respiratory chain [4]. A class of fungicides (SDHIs) can also be attacked by the SDH. Resistance to the SDHI boscalid, an ingredient of the premix fungicide pristine, first appeared in 2011 [5, 6]. SDHI is a category of fungicides that effectively manage fungal diseases in agriculture and gardening, especially in cherry crops. Unfortunately, resistance to SDHIs [6] has increased in various pathogenic fungi, leading to fruit diseases. Understanding the chemical mechanisms of fungicide resistance enables us to develop resistance management approaches.

Two different mechanisms concerning SDHI resistance have recently been discussed among researchers. These boscalid-resistant *B. jaapii* fungi consist of the H260R mutation in the SdhB genome (B-H260R) [5] and mutation of Histidine residue to either Arginine or Tyrosine is completely usual among other boscalid-resistant fungi [6–8]. It is notable that it can be produced due to unusual, repeated usage of pristine in any cherry garden. SDHI through 4 genes, consisting of SdhA (SDHI complex flavoprotein subunit A), SdhB (SDHI complex iron-sulfur subunit B), SdhC (SDHI subunit C), and SdhD (SDHI complex subunit D), create a ubiquinone-bonding pocket. The SDHI target genes, SdhB, SdhC, and SdhD, mutations provide resistance to SDHIs. Moreover, overexpression of ABC transporters plays an essential role in reducing sensitivities to all types of SDHI fungicides.

These types of packages are centers affected by SDHI fungicides, and several mutations appear in their structure due to SDHI resistance [5]. Meanwhile, due to the diversity of biochemical compounds of SDHI fungicides, mutations such as B-H277Y and B-H277R, which restructured the organization of the ubiquinone-binding package and controlled boscalid from creating a reaction of the SDH with other SDHI [6] fungicides (for instance, Fluopyram)

[9]. Fluopyram or *N*-{2- [3-Chloro-5- (tri-fluoro-methyl) pyridin-2-yl] ethyl}-2-tri-fluoro-methyl benz-amide; (Figure 3-a) is a fungicide applied in agriculture as an inhibitor of SDHI. It is also used to control fungal diseases such as gray mold (Botrytis Cinerea), powdery mildew, apple scab, Alternaria, Sclerotinia, and Monilinia.

Recently, several papers concerning the mechanism of resistance to fluopyram and fluxapyroxad (Figure 3-b) have been published [10–18], as well as various Sdh gene mutations have been recognized that are able to produce complex structures with other genomes from fluopyram (As instance C-G91R and C-G150R with fluxapyroxad (3-Difluoromethyl)-1-methyl-*N*-(3′,4′,5′-trifluoro[1,1′-biphenyl]-2-yl)-1*H*-pyrazole-4-carboxamide), resistance in S. homo-eocarpa [15], B-P225F and B-N230I with fluopyram.

Fluxapyroxad is also an SDH inhibitor [12, 14, 15, 18], which interacts with several fungal growths, including spore germination and mycelium. Specifically, it interacts with the production of SDHI and the complex II in the mitochondrial respiratory chain [19], which, in turn, interferes with the tricarboxylic cycle and mitochondrial electron transport, as seen in Cinerea [13] and B-I280V in SdhB [20].

We assumed that the adjacent presence of boscalid-resistant subunits of B. jaapii to fungicides such as fluopyram or fluxapyroxad could quickly lead to resistance to those structures. Meanwhile, it was unknown to us whether these kinds of resistance could be acquired sequentially, i.e., whether B. jaapii strains carrying the B-H260R mutation would evolve a second mutation conferring resistance to fluopyram and/or fluxapyroxad. In this work, we simulated the mechanism of resistance of populations of *B. jaapii* to fluopyram and fluxapyroxad in CLS efficacy.

The amount of resistance of a fungal pathogen decreases disease caused by fungicide-resistant [21], and we also identified mutations in the SdhB and SdhC genes of B. jaapii that confer resistance to fluopyram and fluxapyroxad and are associated with different resistance phenotypes. The genome sequence of *B. jaapii* for recognizing SdhB, SdhC, and SdhD SDHI fungicide target genes has been evaluated by Peng *et al*. [22-24]. They selected twenty-two *B. jaapii* with different levels of sensitivity to boscalid, fluopyram, and fluxapyroxad for analysis. They also used the initial primers of the *B. jaapii* SdhB, SdhC, and SdhD genes and their sequences (Table 1).

Table 1. Amplification and sequencing of Oligonucleotide primers [22].

Target	Sequence (5'- 3')
SdhB	CCCAATAAGACACCTCAACTC
	ATAACACTCTCGCATCCCTA
	GGTTGATCCGACGTTGAC
	GTACGGCTTGATGGACTTG
SdhC	ATGTTGGCTCAACGAGCTG
	CTAATACGCCAATGCCAAGTAC
	CTGCTGCCTTTGAGGATAG
	GCTTGTAGATGGAGAGGTTG
SdhD	ATGGCATCAATTGTGCGAC
	CTATGCCGCCCAGATCCT
	TTCCCGGTTCCTTGAGAGT
	CCGTGGGAATGTAGTCGATTATG

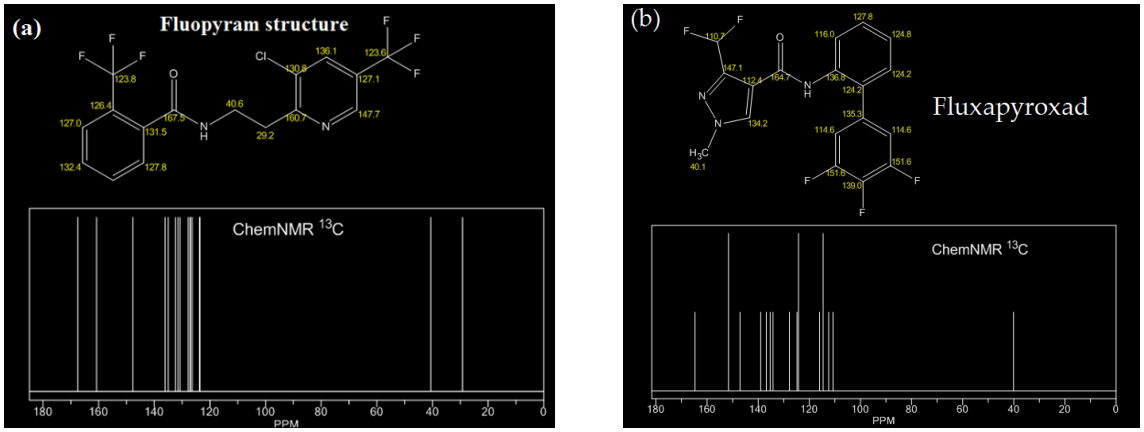

Figure 3. NMR structures of **(a)** Fluopyram; **(b)** Fluxapyroxad.

2.2. Powdery mildew symptoms.

This fungus is a biotrophic pathogen and grows as superficial hyphae that cause haustoria in epidermal cells of green grapevine tissue and consists of two genetic strains, A and B. Group A has flag shoots in an epidemic, and group B is associated with flag shoots and ascospores infection, which is more epidemic than group A. *E. necator* overwinters as mycelia and conidia in dormant buds and as chasmothecia on the bark of the trunk and cordons (Figure 4)

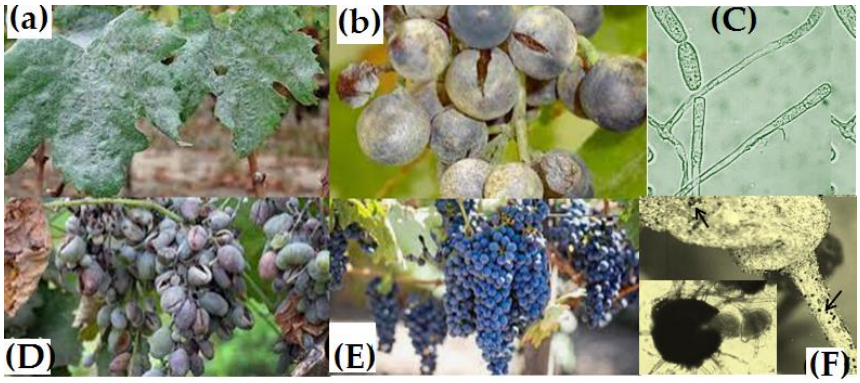

Figure 4. (a) Powdery mildew symptoms, white powder on the upper leaf surface **(b)** on grape **(c)**; (d) Chasmothecia with immature conidiophores; **(e)** conidia on grape; **(f)** a microscopy image of Powdery mildew

During rain around 2.5-3mm and with temperatures above 12°C, Chasmothecia is able to produce ascospores that infect leaves adjacent to strings, causing PM colonies. Consequently, the Conidia are dispersed through the wind and initiate multiple infections on green tissues during the growing season. Grapevine powdery mildew is a serious problem worldwide, affecting both cultivated gardens and wild forests, causing human disease and economic losses. This fungus belongs to the *Erysiphe necator* Schwein, an obligate biotrophic fungus belonging to the family Erysiphaceae [25].

The mildew colonies that grow epiphytically appear whitish and powdery. The pathogen can infect all green parts of the plant, including leaves, shoots, flowers, and bunches; however, infection of the flowers is the most common issue [25, 26], leading to flower drop and, consequently, reduced berry production. In addition to these issues, the infection reduces photosynthesis and lowers sugar and anthocyanin levels in grape juice, resulting in a less intense color. At the same time, it increases acidity and raises the concentrations of phenylacetic and acetic acids, ultimately leading to poorer wine quality [26–30]. Most grape varieties of the *Vitis vinifera* family lack genetic resistance to Grapevine powdery mildew and

are therefore highly susceptible to infection by Erysiphe necator [31–33]. It is notable that, compared with any fruits, viticulture is one of the highest users of fungicides (an average yearly use of 20 kg/ha of pesticides) [34], which causes a reduction in resistance against E. necator in different cultivation areas, such as on the Sultan seedless vineyards in the Aegean region located in western Türkiye [35].

According to the Fungicide Resistance Action Committee (FRAC) classification index [36], a complete list of Fungicides for controlling Grapevine Powdery Mildew and reducing resistance of E. necator powdery mildew to pesticides and fungicides [37] belonging to different chemical classes is presented in Table 2. Some of them are fungicides targeting protein enzymes that participate in the mechanism of electron transport within the mitochondrial membrane and sterol biosynthesis. Some other classes can be included as Sterol biosynthesis inhibitors (SBI), de-methylation inhibitors (DMI), MBC-fungicides (Methyl benzimidazole carbamates or Benzimidazoles), SDHI, QoI (Quinone outside Inhibitors), or SBI, and Hydroxy-2-amino-pyrimidine (HAP) fungicides, which consist of fungicides with a broad spectrum of activities used against different groups of pathogens.

Table 2. Fungicides employed against grapevine powdery mildew are categorized according to the Fungicide Resistance Action Committee (FRAC), with documented cases of resistance observed in *Erysiphe necator*.

Action	Active site	Chemical compound	FRAC-Index	Item instance	Reference
Cytoskeleton and motor protein	β-tubulin of microtubules	Benzimidazoles fungicides	1	Thiophanate- methyl	[46]
Cytoskeleton and motor protein	myosin	Aryl phenyl- ketones	50	Metrafenone, Pyriofenone	[45]
Respiration	succinate dehydrogenase	SDHI	7	Boscalid, Fluopyram, Fluxa-pyroxad	[47]
Respiration	cytochrome	QoI-fungicides	11	Pyraclostrobin Trifloxystrobin	[48]
Signal transduction	Signal transduction	Azanaphthalenes	13	Proquinazid	[49]
Sterol biosynthesis	sterol biosynthesis	SBI	3	Difeconazole Fenbuconazole Tetraconazole Triadimef	[50,51]
Nucleic acid metabolism	Adenosin-deaminase	HAP	8	Bupirimate	[51,52]

2.2.1. MBC (FRAC index=1).

Properties of MBC or Benzimidazoles (Scheme 1) were discovered gradually in the decade of 1960-1970 and exhibited the high-quality fungicides, which are used basically for foliar diseases as well as for seed dressing at low rates [38,39]. MBC fungicide action was distinguished in 1973 by Davidse *et al*. [40]; they prevent β-tubulin of microtubules assembly during polymerization of the nuclear division, germ tube elongation, and mycelium growth. In many countries in Europe and the Middle East, resistance to MBC has been observed in over 100 fungal species, including various powdery mildew species. [37, 41]. Although several mutations in the β-tubulin subunits have been identified in laboratory studies, the most significant are E198A/G/K/Q and F200Y [39]. These mutations are noteworthy because, while they are not directly related to MBC itself, they alter the secondary structure of β-tubulin, thereby preventing fungicide binding. [42].

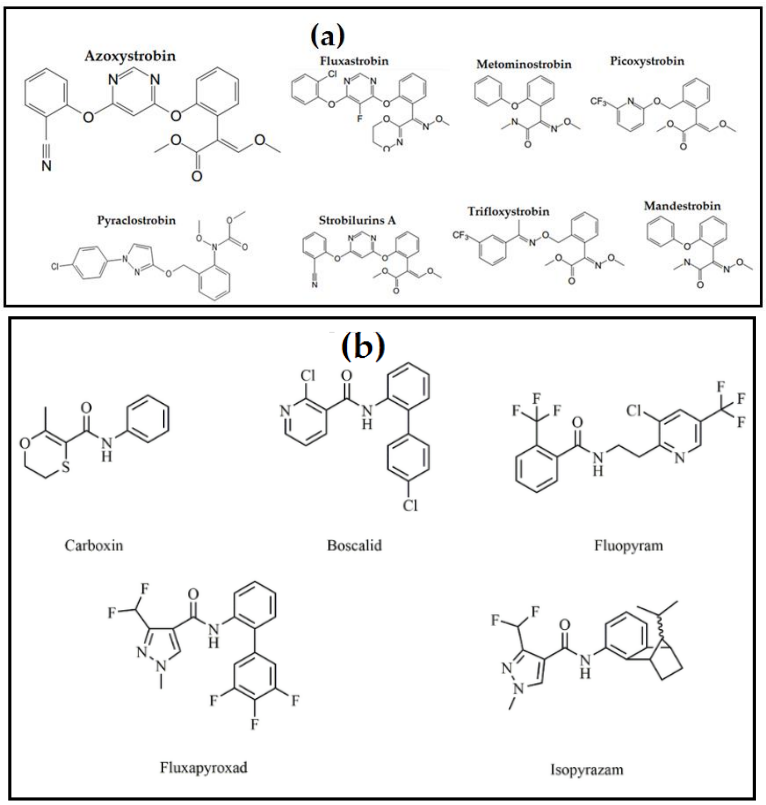

Scheme 1. (a) Molecular structures of strobilurins; **(b)** Molecular structures of SDHI.

2.2.2. Aryl-phenyl ketones fungicides (FRAC index=50).

Aryl-phenyl ketones, exclusively, are used for powdery mildew as a fungicide and pesticide, and consist of a strong fungicide known as Metrafenone. Studies on powdery mildew have shown that concentrations around 1250 mg/L [43-45] can disrupt the actin cytoskeleton and interfere with hyphal morphogenesis and polarized hyphal growth.

2.2.3. QoI- fungicides or Strobilurins (FRAC index=11).

QoI, which is registered for use in agriculture [48], investigated a revolution in fungicide drugs and commercial activities in bazaars, and it still belongs to the best-selling products derived from natural compounds known as Strobilurins A. This fungicide acts within the inner mitochondrial membrane by binding to the quinol oxidation site (Qo) of cytochrome bc1 [53-55]. The mechanism of action is based on the disruption of electron transfer between cytochrome cyto-bc1, which, as a result, halts the ATP synthesis. Currently, a series of Strobilurin fungicides, including azoxystrobin, pyraclostrobin, fluoxastrobin, kresoxim-methyl, trifloxystrobin, picoxystrobin, mandestrobin, and metomino-strobin, were synthesized [56] (Scheme 1).

2.3. Materials and methods.

2.3.1. Docking simulation.

BIOVIA-2020's docking software, Chem-3D, HyperChem, Visual Molecular Dynamics (VMD), and the Chemistry Harvard molecular mechanics (CHARMM) software have been used for all molecular minimization and Gibbs energy calculations from molecular docking. Molecular docking methods have been used to distinguish how the mutations bind the

QoI fungicides to the Qo-binding pockets. We are seeking to understand the mechanism of QoI fungicide resistance, which may help us identify more potent inhibitors of plant diseases without destroying forests, rivers, and our ecological systems. We designed and docked several QoI fungicides to the Qo-active site through various mutations, including G143A, F129L, and G137R (Figure 5).

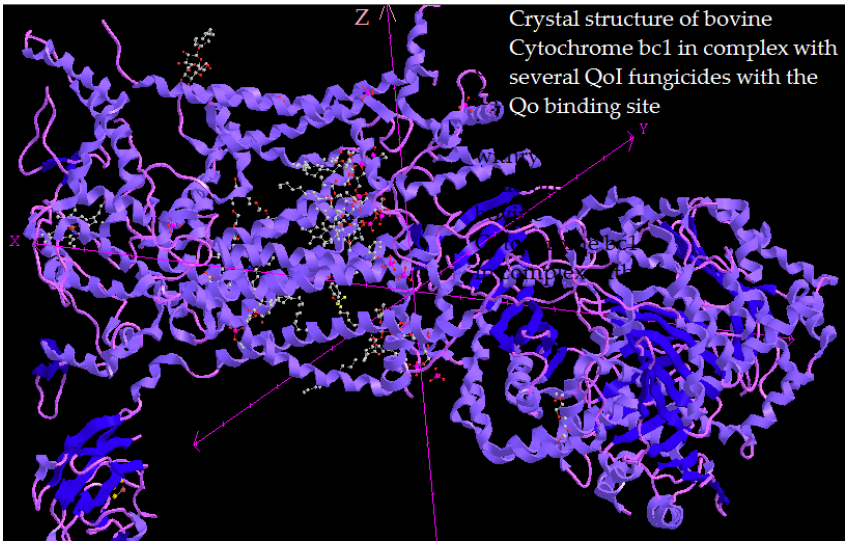

Figure 5. 1SQB crystal structure analysis of bovine cty-bc1 with Azoxystrobin.

2.3.2. Design of hybrid compounds.

In this work, the design of dual inhibitors combining SDHIs and commercial strobilurins was aimed at providing several compounds with appropriate sizes and geometries to achieve optimal docking of both enzymes [57, 58]. All QoI fungicides share a common structural feature consisting of a methyl-(E)-β-methoxyacrylate pharmacophore linked to a phenyl ring. The group side branches are generally demonstrated by an aryl-oxy or an aryl-oxy-methyl [59]. In other words, although SDHIs have different structures, all of them exhibit a general section in their structure as the amide bond, which is bonded to an aromatic or heterocyclic ring. The core segment is important for in vivo activity, which enters strongly into the active site of SDH. The attached linker to the amine group is an alkyl group containing an aromatic substituted (or sometimes substituted) heterocyclic group. In the ortho situation, the hydrophobic agent is an additional ingredient of the other molecule [60]. Considering these approaches, we proposed simulating the β-methoxyacrylate moiety of strobilurins and replacing it with a suitable aromatic amide at a suitable position in SDHIs. As mentioned above, the first-generation hybrid structures consist of three rings of azoxystrobin with methyl-(E)-β-methoxyacrylate strobilurins attached via a carboxamide pharmacophore, as in three commercial SDHI inhibitors. We are looking to reach highly active enzyme pharmacophore structures that enable overcoming strobilurins resistance; therefore, for highly strong interaction with protein enzymes, the following should be considered in any design for molecular dynamic simulation: 1-Spatial position of the two pharmacophores; 2- Nature of the linker; 3-substitution pattern of the SDHI (Figure 6).

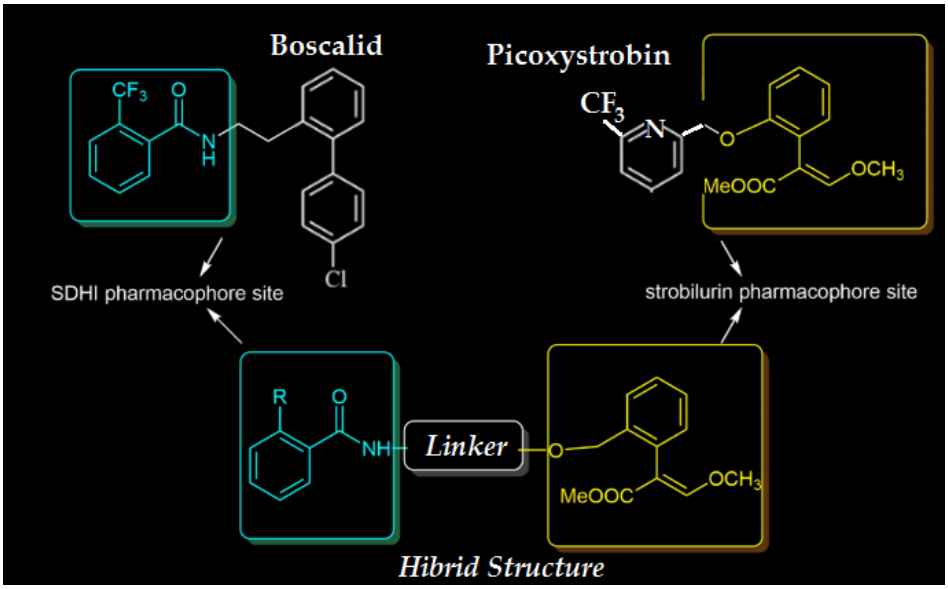

Figure 6. Merging of SDHI with various strobilurins.

3. Results and Discussion

3.1. Cytochrome bc1 and binding modes as the resistance mutation.

Cytbc1 is an important target for vegetable and fruit (especially grape) fungicides, as Qo-site inhibitors (QoIs) can control a wide range of plant pathogenic fungi from the ascomycetes, basidiomycetes, and oomycetes families. Cytochrome bc1, as a fungicide enzyme in crop pathogens plant disease control, is a unique item in pharmacy due to different modes of action and goals, including fungal sterol biosynthesis inhibitors and cytbc1 inhibitors. The cytochrome bc1 complex is part of the mitochondrial respiratory chain in several pathogenic eukaryotic microorganisms, especially those causing crop diseases. Cytochrome bc1 consists of two quinone /quinol-binding sites that can control fungicidal agents. The QoIs on the bazar consist of several synthetic strobilurins, such as azoxystrobin and fluoxastrobin, which can share the same binding mode as the resistance mutation G143A in the cytbc1. Unfortunately, its performance was quickly challenged due to the resistance of many pathogens, such as powdery mildew [60] and *Plasmopara viticola* [7]. Fungal phytopathogen resistance to azoxystrobin was discovered to be caused by the cytcb1 mutation G143A in the Qo site (Figure 7), and A143 was discovered later in cytcb1 of the strobilurins-producing *Mycena galopoda* [56]. Based on FRAC information, the G143A substitution has now been listed among over twenty species of phytopathogen fungi. The G143A mutation creates a large amount of resistance that causes an increase in disease. Evaluating cytbc1 with the linkage of azoxystrobin confirms a rearrangement of G143 by alanine of the fungicide, and also, G143A considerably increases resistance to azoxystrobin without any effect on cytbc1activity. This large amount of resistance could explain the fast spread of G143A in many fungi. Three other cytcb1 mutations have also been observed, such as F129L, which was created in Barley net blotch, and G137R, which was found in isolates of Pyrenophora, and G137S, found in pecan scab (Figure 7) [61]. The side chain of F129 is directed to a hydrophobic hole, which causes access to Qo. Therefore, this mutation has little effect on enzyme activity but decreases its sensitivity to the QoI azoxystrobin and stigmatellin [62, 63].

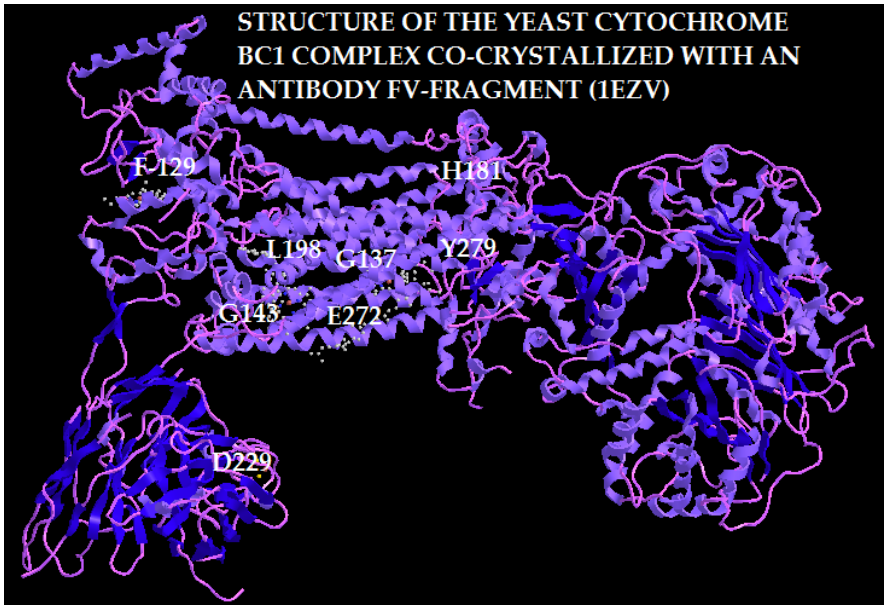

Figure 7. Atomic structure of cytcb1 interaction with antibody.

3.2. Resistance mutations and alternative fungal pathogens of QoI/QoI.

The binding situation of kresoxim-methyl, azoxystrobin, pyraclostrobin, fluoxastrobin, trifloxystrobin, picoxystrobin, mandestrobin, and metominostrobin to bovine heart CYTBC1 (Figure 5) extracted from the docking Gibbs energy data has been listed in Table 4. The proper docking simulation could be useful for studying the Gibbs energy of these QoI fungicides to the active site. Mutations associated with QoI- resistance in the cytochrome-bc1 gene in plant pathogens are able to control resistance to Qo inhibitors, consisting of 1- changing position from Gly to Ala from 143 (G143A), 2-changing from Phe to Leu from 129 (F129L), 3-changing from Gly to Arg from 137 (G137R). The methoxy acrylate groups of these strobin structures of QoI fungicides merged between the residues F129L and G137R of the C-helix, and hydrogen bonds, π- π stacking, and van der Waals interaction from QoI fungicides attached to the Qo-active site. In addition, azoxystrobin from the 1SQB protein data bank (Figure 5) has been selected for docking. For all the above-mentioned processors, molecular docking was performed using the ab initio-optimized small molecules in the Drug Discovery Suite [64]. The QoI binding active site of the cytochrome bc1 was distinguished through the presence of azoxystrobin transferred from the bovine cytochrome bc1 complex (1SQB [65]). Molecular docking was accomplished by its extra precision (XP) form [66–68]. For the docking system, our model of the cytochrome bc1 complex was drawn through visual molecular docking and also by Chem-3D. The energy minimization has been done via Charmm software, and we also used the BioLuminate Protein Preparation Wizard with the OPLS3e [69, 70] force field. The binding free Gibbs energy of all complexes generated by our molecular docking pipeline was calculated using both Glide XP Score and Prime MM-GBSA, which combines molecular mechanics with a generalized Born and surface area scoring function [62]. RFs caused by F129L and G137R are usually placed between 6-16, and sometimes around 45, and also resistance factors from G143A are in most items more significant than 100. Isolates carrying G143A express high resistance, and f isolates with F129L or G137R express medium resistance. G143A is responsible for QoI resistance in more pathogen species than F129L because 20 genotypes out of 26 plant pathogens carry G143A.

3.3. Sensitivity of double mutation to SDHI.

Based on several commercial reports, Bingxue *et al*. [71] confirmed that carboxin, boscalid, fluopyram, and penthiopyrad are the most sensitive to SDHI fungicides among other compounds. Several double mutations were measured through experimental testing. They exhibited solid double strong double mutations resistant to boscalid. The potency of these compounds (which refers to the concentration that induces a response halfway between the baseline and maximum) should be expressed as the half-maximal effective concentration (EC50) listed in Table 3 (rounding numbers) [71]. Nevertheless, the EC50 amounts were different among the double mutations. The double mutations B-I280V+D-D95E, B-H278R+D-D95E, and B-H278Y+D-G109V were categorized as normal resistance (MR), with EC50 values ranging from 2.472~4.062 µg/mL. However, three double mutations, including the B-H278Y+DD95E, B-I280V+D-G109V, and D-B-H278R+ D-G109V genotypes, were distinguished to high resistance (HR, EC50 values: ~13.9~16.8µg/mL). The EC50 values of B-I280V+D-H105R were >25 µg/mL and were identified as conferring very high resistance (VHR).

Table 3. Sensitivity of *C. cassiicola* to SDH inhibitor fungicides.

Strain or Mutants	EC50 (µg/mL)			
	Carboxin	**Boscalid**	**Floupyram**	**Penthiopyrad**
B-I280V	29.6 (13.4)	0.4 (2.7)	6.5 (33.8)	1.47 (15.8)
B-H278R	34.1 (15.5)	3.4 (22.9)	0.17 (0.870)	0.6 (6.6)
B-H278Y	18.3 (8.2)	38.3 (255.4)	0.03 (0.150)	2.3 (24.6)
D-D95E	8.1 (3.7)	1.4 (9.5)	2.8 (14.3)	1.7 (17.9)
D-H105R	9.9 (4.5)	4.3 (28.6)	4.3 (22.4)	11.1 (119.7)
D-G109V	18.0 (8.1)	3.2 (21.6)	12.0 (61.7)	3.7 (40.1)
B-I280V+D-D95E	31.4 (14.2)	4.0 (27.0)	6.7 (34.50)	6.1 (65.8)
B-H278R+D-D95E	29.0 (13.1)	3.0(19.9)	0.26 (1.36)	0.36 (3.9)
B-H278Y+D-D95E	25.0(5.5)	13.9 (43.7)	1.5 (13.7)	1.5 (19.3)
B-I280V+D-G109V	36.8 (16.6)	16.8 (112.1)	6.8 (35.2)	20.1 (216.1)
B-H278R+D-G109V	53.3 (24.1)	17.0 (113.4)	3.7 (19.2)	8.2 (87.9)
B-H278Y+D-G109V	20.6 (9.3)	2.5 (16.5)	7.6 (39.3)	2.0 (22.2)
B-I280V+D-H105R	28.909 (13.06)	26.827 (178.8)	25.158 (130.3)	18.345 (197.2)
The synergistic activity of the combination of different single-point mutations in SDHI *resistance				
Double Mutation	**Carboxin**	**Boscalid**	**Fluopyram**	**Penthiopyrad**
B-I280V+D-D95E	1.67	4.42	1.43	3.90
B-I280V+D-G109V	1.55	9.20	0.74	7.73
B-I280V+D-H105R	1.46	11.40	4.64	2.91
B-H278R+D-D95E	1.37	1.23	0.18	0.31
B-H278R+D-G109V	2.05	5.10	0.61	3.76
B-H278Y+D-G109V	1.14	0.12	1.27	0.68
B-H278Y+D-D95E	1.89	0,70	1.10	0.76

*Synergistic coefficients (SC)

3.3.1. Analysis of Synergistic Coefficients (SC).

The synergistic coefficient (SC) was calculated using the following approach: first, the actual EC_{50} (AE) values were normalized to a reference isolate according to the following formulas:

$AE(A) = \frac{EC50(A)}{EC50(A)} = 1$; for the mutation A and then , $AE(B) = \frac{EC50(B)}{EC50(A)}$ for the mutation B. Consequently actual EC_{50} of a double point mutation (A + B) can be measured by $AE(A + B) = \frac{EC50(A+B)}{EC50(A)}$. Theoretical EC_{50} (TE) of a double point mutation (A + B) can be estimated through: $TE(A + B) = 0.5 \times AE(A) + 0.5 \times AE(B)$, and finally, the synergistic coefficient

was determined as: $SC = \frac{AE(A+B)}{TE(A+B)}$. Based on synergistic coefficients and the activity of the combination of different single point mutations in SDHI resistance, the combination was categorized into 3 groups: synergic effects (SC > 1.2), additive effects (0.8 ≤ SC ≤ 1.2), and antagonistic effects (SC < 0.8). The statistical resistance from SDHI amounts was evaluated according to the log (EC50) values. Linear regression revealed no considerable resistance between fluopyram and boscalid (rs = 0.551, p = 0.157), fluopyram and carboxin (rs = 0.263,p = 0.528), or carboxin and boscalid (rs = 0.699, p = 0.054), while a tight association was observed between penthiopyrad and all the SDHIs tested (carboxin: rs = 0.713, p = 0.040; boscalid: rs = 0.838, p = 0.009; fluopyram: rs = 0.786, p = 0.021). Synergistic coefficients were calculated to quantify the combined effects of dual-action SDHI–QoI fungicides and microbial bio-fungicides. Statistical analyses, including ANOVA and regression, were performed to validate the significance of observed synergistic interactions. Docking simulations were used in parallel to predict binding affinities of individual and combined compounds, allowing correlation between in silico binding energies and experimentally or theoretically derived synergistic coefficients.

3.4. Docking simulations result.

Our results have been extracted from molecular simulations based on our previous work using first-principles calculations, molecular modeling, molecular mechanics, and docking. Consequently, we designed and calculated each part of the molecular simulation using a QM/MM method, including ONIOM input files throughout the manuscript [72-93]. The QM/MM approach is a hybrid computational methodology that combines quantum mechanics (QM) for the chemically active region of a system with molecular mechanics (MM) for the surrounding environment. This allows accurate modeling of electronic structure and reaction mechanisms in the active site while maintaining computational efficiency for large biomolecular systems. The ONIOM (Our own N-layered Integrated Molecular Orbital and Molecular Mechanics) method is a specific implementation of QM/MM that divides the system into multiple layers. A high-level QM layer treated with ab initio or DFT methods for the reactive center. A low-level MM layer treated with force fields (e.g., AMBER, MMFF94) to describe the surrounding protein or solvent. ONIOM calculations enable geometry optimization, energy evaluation, and reaction pathway analysis of complex systems by balancing accuracy and computational cost. In this study, ONIOM was applied to investigate the interactions of dual-action SDHI–QoI fungicides with fungal target sites, enabling precise estimation of binding energetics and electronic effects within the active site while accounting for the influence of the surrounding macromolecular environment.

Through dual activity via docking simulations, we are able to explore the binding modes of the novel molecules to both the Cytcb1 subunit and the SDHI fungicide. In both items, the enzymes were modeled using simulation methods, and the docking simulation data were analyzed by comparing them with known ligands. The Cytcb1 models were generated from the primary sequence, and the two sequences are substantially identical over the relevant range of residues. Therefore, their structures were modeled by using the resolved Cytcb1in complex (PDB ID: 1EZV) with the inhibitor as the template (Figure 7). The SDHI fungicide consists of four subunits that must be linked, and the active site for attaching them is located at the center of the interface. We simulated our model using several subunits based on three

primary sequences: G4NE44, L7JQS7, G4N2P5, and Q5G5B2. Consequently, different SDHI fungicides were generated according to the docking simulations with Cytcb1. Dual pesticide combinations containing SDHI and QoI are listed in Table 4.

Table 4. Various merging of strobilurins by SDHI compounds through a dual combination.

Synthetic Strobilurins	SDHI			Linker	Dual pesticides combination
	Chemical group	Common name	Formula		
(a): Azoxystrobin	Phenyl-benzamides	(a'): Benodanil (b'): Flutolanil (c'): Mepronil	$C_{13}H_{10}INO$ $C_{17}H_{16}F_3NO_2$ $C_{17}H_{19}NO_2$	Phenyl-benz-amides pharmacophore site -AzoxyStrobin pharmacophore site	a-a' a-b' a-c'
(b): Trifloxystrobin	Pyrazole-carboxamides	(d'): Benzovindiflupyr (e'): Bixafen (f'): Fluindapyr (g'): Fluxapyroxad (h'): Furametpyr (i'): Inpyrfluxam (j'): Isopyrazam (k'): Penflufen (l'): Penthiopyrad (m'): Sedaxane	$C_{18}H_{15}Cl_2F_2N_3O$ $C_{18}H_{12}Cl_2F_3N_3O$ $C_{18}H_{20}F_3N_3O$ $C_{18}H_{12}F_5N_3O$ $C_{17}H_{20}ClN_3O_2$ $C_{18}H_{21}F_2N_3O$ $C_{20}H_{23}F_2N_3O$ $C_{18}H_{24}FN_3O$ $C_{16}H_{20}F_3N_3OS$ $C_{18}H_{19}F_2N_3O$	Pyrazole-carboxamides pharmacophore site -Trifloxystrobin pharmacophore site	b-d' b-e' b-f' b-g' b-h' b-i' b-j' b-k' b-l' b-m'
(C): Kresoximmethyl	Ethyl thiophene amide	(n'):Isofetamid	$C_{20}H_{25}NO_3S$	Ethyl thiophene amide pharmacophore site - Kresoximmethyl pharmacophore site	c-n'
(d): Pyraclostrobin	Pyridinyl-ethy benzamide	(o'): Fluopyram	$C_{16}H_{11}ClF_6N_2O$	Pyraclostrobin pharmacophore site - Pyraclostrobin pharmacophore site	d-o'
(e):fluoxastrobin	Furan-carboxamides	(p'): Fenfuram	$C_{12}H_{11}NO_2$	Furan-carboxamides pharmacophore site - fluoxastrobin pharmacophore site	e-p'
(f):oryzastrobin	Oxathiin-carboxamides	(q'): Carboxin (r'): Oxycarboxin	$C_{12}H_{13}NO_2S$ $C_{12}H_{13}NO_4S$	Oxathiin-carboxamides site - oryzastrobin pharmacophore site	f-q' f-r'
(g): dimoxystrobin	Thiazole-carboxamides	(s'):T hifluzamide	$C_{13}H_6Br_2F_6N_2O_2S$	Thiazole-carboxamides site - dimoxystrobin pharmacophore site	g-s'
(h): picoxystrobin	Phenyl-cyclobutyl pyridineamide	(t'): Cyclobutrifluram	$C_{17}H_{13}Cl_2F_3N_2O$	Phenyl-cyclo-butyl pyridineamide site - picoxystrobin pharmacophore site	h-t'

Since the increasing usage of SDHI, the resistance caused by multiple mutations in the active site of the genome is becoming a serious risk. To evaluate the sensitivity of these mutations to SDHI, we simulated and analyzed the replaced inhibitors using molecular modeling (as shown in Table 5) to confirm the results. A parallel docking study of QoI fungicides in the Qo-binding pocket was accomplished. The crystal structure of the cyto-bc1 enzyme was extracted from the Protein Data Bank (PDB=1SQB) (Figure 5). Sequences were distinguished using an enzyme complex in DNAMAN, and 1SQB PDB was used as a template to study the binding conformations of four novel QoI fungicides within the Qo binding pocket. The three-dimensional structures of several QoI fungicides were first optimized using the MMFF94 force field with MMFF94 charges. These optimizations were performed using the Sybyl 7.3 software package on a Linux platform [36, 94]. Docking testing was performed using the Surflex-Dock method in Sybyl 7.3. A suitable ligand from the viewpoint of negative energy has been chosen according to the top Surflx-Dock energy score [94]. Docking calculation data

of all multiple mutations information are listed in Table 5 and Figures 8 and 9. It is notable that the MMFF94 force field was selected for fungicide docking because it is parameterized for small organic molecules, provides reliable geometry optimization for ligands with aromatic and heterocyclic systems, is computationally efficient, and is compatible with docking software. Accurate ligand geometries from MMFF94 ensure meaningful docking poses and binding energy predictions, which are critical for evaluating dual SDHI–QoI fungicide designs.

Table 5. Docking calculation data of all multiple mutations information with 1ezv.pdb.

Sample	Energy Kcal/mol	VDW Kcal/mol	H-bond Kcal/mol	Docking fitness Kcal/mol
a-a’	-122.7	-109.1	-3.7	-102.9
a-b’	-80.1	-79.1	-1.8	-77.21
a-c’	-89.8	-80.1	-9.7	-85.9
b-d’	-72.5	-69.5	-1.5	-36.3
b-e’	-79.3	-75.8	-3.5	-78.3
b-f’	-69.6	-67.4	-4.5	-66.5
b-g’	-99.5	-91.2	-5.3	-88.3
b-h’	-87.3	-82.7	-6.3	-81.4
b-i’	-88.9	-81.1	-5.4	-79.5
b-j’	-112.4	-101.2	-6.7	-93.6
b-k’	-95.4	-91.4	-7.7	-89.1
b-l’	-88.8	-87.2	-6.7	-84.8
b-m’	-102.5	-97.4	-8.1	-94.7
c-n’	-78.5	-72.4	-6.3	-70.6
d-o’	-87.3	-85.3	-7.3	-84.7
e-p’	-99.5	-94.9	-5.7	-93.8
f-r’	-105.8	-104.3	-8.9	-98.9
f-q’	-97.8	-94.8	-6.7	-93.1
g-s’	-86.7	-81.7	-5.6	-80.5
h-t’	-127.1	-113.6	-13.5	-126.3

Mutation G142A/G142S alters the fungicide binding site, causing the fungicide molecules to be displaced from the amino acid residue at positions 79 to 274 in aa', 134 to 180 in a-b', 78 to 248 in a-c', 79 to 256 in h-t', 41-188 in b-d', and 80 to 248 in be' (Figure 8). In this case, the hydrogen bond is lost and π–π stacking interactions become weak or may even disappear. As a result, van der Waals interactions become more prominent (Table 5). When this site is mutated to alanine (A) or serine (S), the van der Waals surface area increases, indicating greater steric hindrance. This increase likely weakens fungicide binding and leads to high resistance to QoI fungicides (RF > 100).

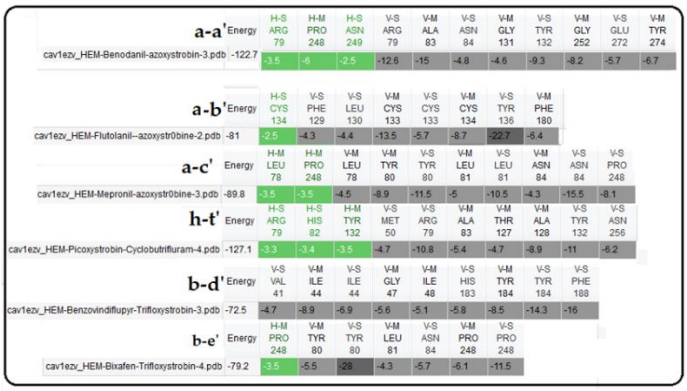

Figure 8. Position of involved amino acids during the merging of strobilurins with SDHI compounds through a dual combination.

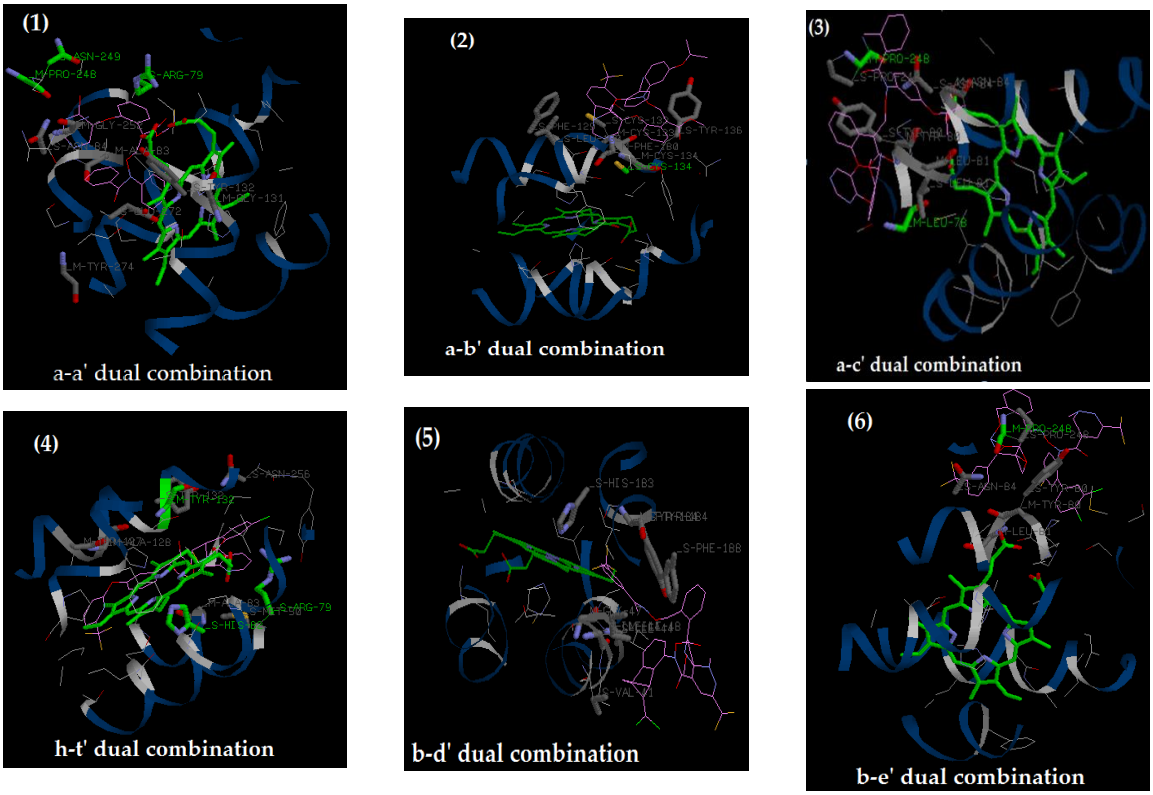

Figure 9. 3D representation of QoI fungicides in the docking pocket of Qo with mutations by docking simulation of SDHI and strobilurins merging through molecular biology and microbial bio-fungicides according to Figure 6 and the table.

Figures 5-7 showed docking results for several compounds with tight binding to azoxystrobin in cytochrome bc1 (PDB ID: 1EZV) [21], where the pharmacophore is near the G143 protein residue (Figure 5). In addition, in both azoxystrobin and SDHI compounds, Phe129 plays a stabilizing role through the formation of a π- π stacking interaction with the aromatic ring distal to the methoxy-acrylic function. Finally, docking results can be interpreted thermodynamically using the predicted Gibbs free energies of binding (ΔG). A more negative ΔG reflects a more favorable balance of enthalpic and entropic contributions upon binding, indicating that the hybrid SDHI–QoI molecules are thermodynamically predisposed to interact strongly with the active site. This supports the observed enhancement in predicted inhibitory activity and rationalizes the improved performance of certain positional isomers and substituted structures. Moreover, differences in ΔG between wild-type and resistant mutants correlate with reduced binding affinity in the mutant enzymes, providing a molecular explanation for resistance.

3.5. NMR and NICS results.

Nucleolus-independent chemical shifts (NICS) are the negative of magnetic shielding, which is computed at a point of interest in molecular space. NICS was first suggested by Michael Bühl *et al*. [95]. In 1995, it discussed the electronic currents in fullerenes and was then investigated by Paul Schleyer [96] as the first idea of NICS. NICS has several variants, such as NICS (0) ISO; (0) means that NICS is calculated at the center of an aromatic ring plane of the molecular structures of strobilurins or the molecular structures of SDHI. From ab initio calculations using magnetic command (NMR = GIAO order), the ISO parameters were obtained, which indicate the amount of aromaticity for the mentioned rings in both the

molecular structures of strobilurins and SDHI. The word is generally used to define energetic stability, and although NICS has no direct relationship with stability due to the fact that energetic stability is a ground-state property, negative NICS and strong diamagnetic current density can, in some cases, define the strength of electronic currents for aromaticity amount through the NICS values (Figure 10).

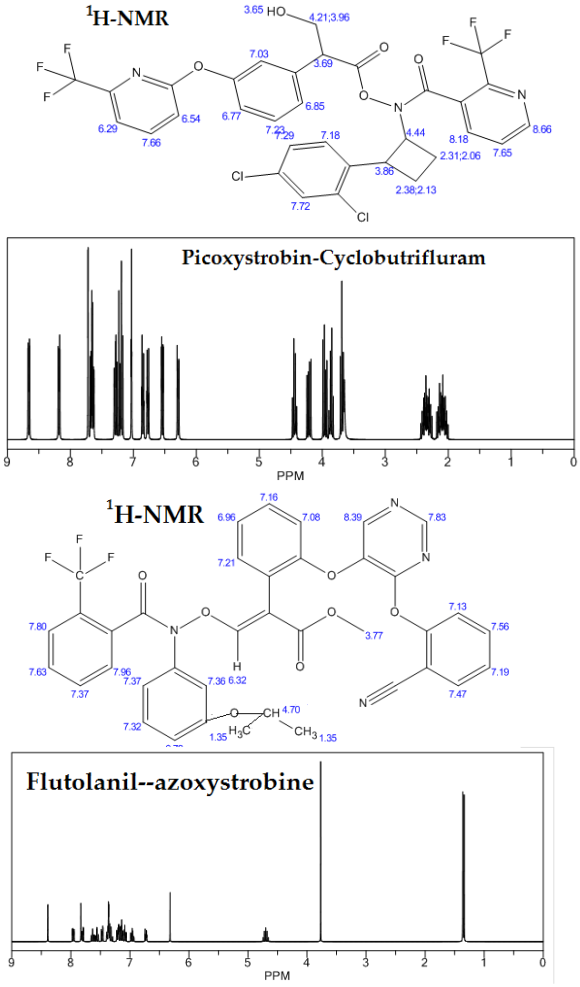

Figure 10. Proton NMR of dual pesticides including h-t' and a-b' using NICS calculation.

3.5.1. Isotropic and anisotropic parameters.

Total chemical shift tensors "**σ**" are non-symmetrical tensors which can be separated through three independent parameters, which are known as isotropic, traceless symmetric, and traceless anti-symmetric. In addition, a spherical tensor has been exhibited by Haeberlen [97], Mehring [98], and Diehl [99]. They have investigated fundamental tensors as:

$$\boldsymbol{\sigma} = \boldsymbol{\sigma}^{iso(0)} + \boldsymbol{\sigma}^{anti(1)} + \boldsymbol{\sigma}^{sym(2)} \quad (1)$$

Spherical tensors can also be written as:

$$\boldsymbol{\sigma}_{\mathbf{0}}^{iso(2)} = \sqrt[2]{\mathbf{3}/\mathbf{2}}\,\boldsymbol{\delta}_{(zz)} \text{ And } \boldsymbol{\sigma}_{\pm\mathbf{2}}^{sym(2)} = \frac{\mathbf{1}}{\mathbf{2}}\boldsymbol{\delta}_{(zz)} \quad (2)$$

Where, $\boldsymbol{\delta}_{(zz)}$ is the reduced anisotropy and can be calculated through:

$$\boldsymbol{\delta}_{(zz)} = (\boldsymbol{\sigma}_{zz} - \boldsymbol{\sigma}_{iso}) = (\boldsymbol{\sigma}_{33} - \boldsymbol{\sigma}_{iso}) \quad (3)$$

This parameter is related to the anisotropy (**Δσ**) with:

$$\Delta\boldsymbol{\sigma} = \frac{\mathbf{3}}{\mathbf{2}}\,\boldsymbol{\delta}_{(zz)} \quad (4)$$

From equations 4 and 5, asymmetry (η) shielding can be estimated as:

$$\Delta\boldsymbol{\sigma} = \boldsymbol{\sigma_{zz}} - \tfrac{1}{2}\left(\boldsymbol{\sigma_{xx}} + \boldsymbol{\sigma_{yy}}\right) \quad (5)$$

$$\boldsymbol{\eta} = \left(\frac{\boldsymbol{\sigma_{yy}} - \boldsymbol{\sigma_{xx}}}{\boldsymbol{\delta_{(zz)}}}\right) = \frac{\mathbf{3}(\boldsymbol{\sigma_{yy}} - \boldsymbol{\sigma_{xx}})}{\mathbf{2}\Delta\boldsymbol{\sigma}} \quad (6)\ [100].$$

The magnetic resonance of the spins is seldom isotropic; they must be represented with new tensors (Herzfeld-Berger notation) [101]. These tensors are known as Span ($\boldsymbol{\Omega}$) $\Omega \geq 0$, which illustrates the maximum width of the model and the skew (κ) of the tensors which are a magnitude of the values:

$$(\boldsymbol{\Omega}) = \boldsymbol{\sigma_{33}} - \boldsymbol{\sigma_{11}}\ \boldsymbol{and}\ \boldsymbol{\kappa} = \frac{\mathbf{3}(\boldsymbol{\sigma_{iso}} - \boldsymbol{\sigma_{22}})}{\boldsymbol{\Omega}} \quad (7)$$

Moreover, the orientation of skew (κ) is given by:

$$\boldsymbol{\kappa} = \frac{\mathbf{3}(\boldsymbol{\sigma_{1so}} - \boldsymbol{\sigma_{22}})}{\boldsymbol{\Omega}}, (-1 \leq \kappa \leq +1) \quad (8)$$

In some items of an axially symmetric tensor ($\boldsymbol{\sigma_{yy}}$ -$\boldsymbol{\sigma_{xx}}$), Might be zero and therefore η = 0. In addition, the asymmetry (η) indicates how much deviation can appear from the axially symmetrical tensors, so the region of "η" is between zero and one ($0 \leq \eta \leq +1$). NICS is a simple method developed by Schleyer and coworkers that estimates the absolute magnetic shielding at the center of molecules. A negative NICS amount indicates aromaticity, and a positive result indicates anti-aromaticity [96]. The amounts of, $\boldsymbol{\sigma_{iso}}, \Delta\boldsymbol{\delta}, \boldsymbol{\Omega}, \boldsymbol{\eta}$, NICS, and S-NICS calculation according to the formula from equations 1-8 are listed in Table 6. In addition, a significant inverse correlation was validated, statistically ($R^2 = 0.82$, $p < 0.01$), indicating that more negative NICS values correspond to more favorable docking energies.

Table 6. Herzfeld-Berger and Haeberlen convention of NMR components with Cam-b3lyp/cc-pvdz of Strobilurins structures.

Synthetic Strobilurins	σ_{11}	σ_{22}	σ_{33}	σ_{iso}	$\Delta\delta$	κ	Ω	η	NICS	S-NICS
Azoxystrobin	5.31	12.54	21.0	12.94	12.07	-0.08	15.69	0.89	-12.94	-11.83
picoxystrobin	4.32	10.54	15.30	10.05	-8.6	0.13	10.98	0.83	-10.05	-10.45
Trifloxystrobin	3.22	12.44	17.63	11.09	-11.81	0.28	14.4	0.65	-11.09	-10.78
Kresoximmethyl	2.97	10.93	16.92	10.27	-10.95	0.14	13.95	0.82	-10.27	-10.88
Pyraclostrobin	5.45	11.28	16.86	11.19	-8.62	0.02	11.41	0.97	-11.19	-10.98
fluoxastrobin	5.99	13.54	16.86	12.13	-9.21	0.389	10.87	0.54	-12.13	-11.23
oryzastrobin	6.77	12.74	15.98	11.82	-7.58	0.29	9.21	0.64	-11.82	-11.21
dimoxystrobin	5.91	13.76	16.05	11.90	-8.99	0.54	10.14	0.38	-11.90	-11.12

3.5.2. Simulation energy, VDW, H-bond, and docking fitness.

Figure 11 exhibits Simulation energy, VDW, H-bond, and docking fitness versus NICS value. Using the slope of this linear curve, we can suggest and simulate suitable pesticides and commercial fungicides for any fruit or vegetable, based on local climate and forestry conditions. The presence of these compounds significantly alters the overall magnitude of exfoliation due to π-π interactions between SDHI and strobilurins merging through the rise of the strong interactions, including π-orbitals of the strobilurins.

Since diatropic ring current (aromatic) and also paratropic current (anti-aromatic) bonding energies, as well as VDW, H-bond, and docking fitness in benzene-like ring planes in strobilurins are a function of structure activities and stability, therefore NICS values could also be connected directly to the strobilurins' structure and their stabilities, consequently to the chemical properties of pesticides and microbial bio-fungicides. Interestingly, we found that this relationship is linear, which can help us define novel fungicide molecules for fruits and

vegetables under forestry climate-changing parameters, including temperature, moisture, and soil pH, in future research (Figure 11).

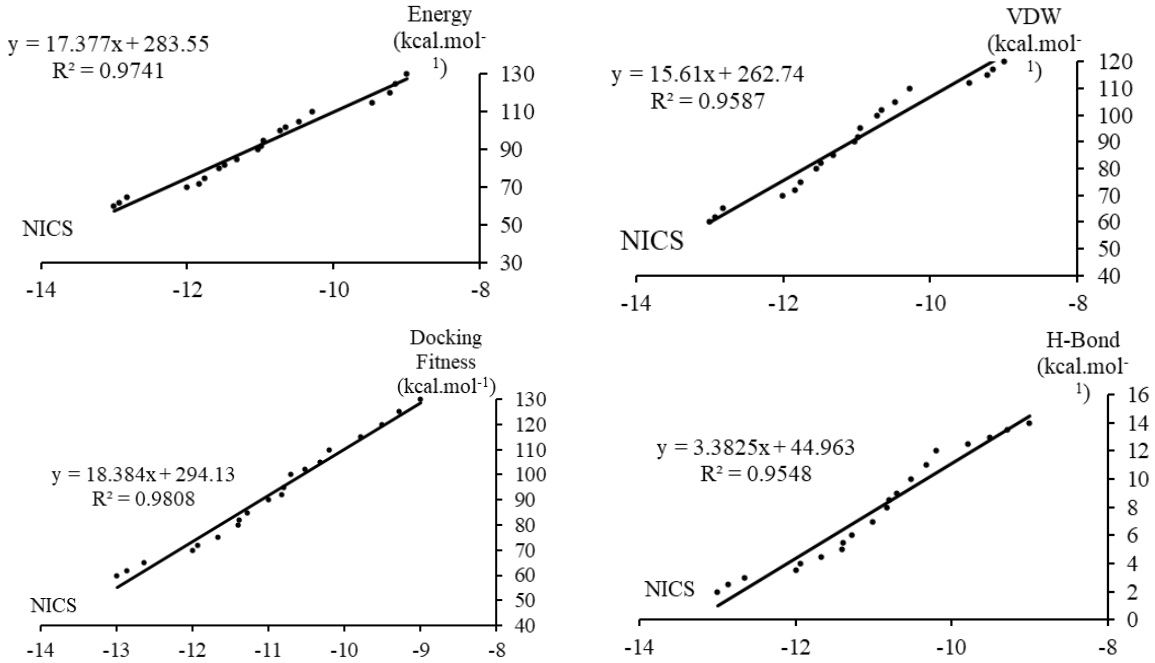

Figure 11. Docking data of all multiple mutations information with 1ezv.pdb from table 5 versus NICS values.

Moreover, critical molecular docking parameters have been explicitly described to ensure reproducibility and reliability of the results. These include the grid box dimensions and center coordinates defining the active site, the exhaustiveness value used during the docking search, validation of the docking protocol through re-docking of the co-crystallized ligand with RMSD evaluation, and the inclusion of appropriate control or reference ligands for comparative analysis.

3.6. Discussion.

Powdery mildew is one of the major fungal diseases affecting several cultivated crops worldwide. Its management relies on commercial fungicides, but resistance poses a threat to food security, and urgent, innovative solutions are needed. In this paper, we presented a structural investigation of new fungicides obtained by combining the pharmacophores of dual pesticides, including SDHI and strobilurin inhibitors, as well as microbial bio-fungicides. This research focused on the structural merging and modification of previous structures to obtain novel versions that enhance antifungal activity against both wild-type and strobilurin-resistant strains. The character of these two pharmacophores and their properties in substitution situations, especially for SDHIs, were investigated to develop a better simulation for suitable activities. We demonstrated that the relative orientation of the dual pesticide combination containing the SDHI and QoI pharmacophores, and the entire shape of the fungicide, strongly impact the biological activity of the hybrid molecule, as shown in Table 5 and Figures 7-10. We found sequencing of the SDHI and QoI in the ortho situation on the central ring yielded high performance in activity against the wild-type strains, and we also discussed the aromaticity of the center of the ring due to this performance as a creator index for better designing and simulation of the dual pesticide combination containing SDHI and QoI pharmacophore. This position indicates that the SDHI pharmacophore suggestion in the ortho

position likely provides a steric obstacle to attaching the QoI pharmacophore to the cytcb1 binding site, while the meta and Para directions are far from any overlap with the binding site. Docking simulation of the mutant type of Qo with QoI fungicides indicates QoI fungicides are bound to a highly hydrophobic surface of Qo (section 2.3.1, figure 5). The DNA sequences of the cty-bc1 genome were compared among the mutants, and three amino acid substitutions (G142A, Y131C, and F128S) were identified in the cytochrome-bc1 protein of various mutants exhibiting high resistance to the novel QoI fungicides. The G143A has been confirmed as the most common item of QoI resistance and has been distinguished in these variants. Our results further confirm that amino acid substitutions at this position are closely associated with the failure of QoI fungicides to control the disease. Another mutation identified in this study, Y131C, confers high resistance to all QoI fungicides (RF > 100). However, this mutation was generated through UV radiation and has not yet been reported in natural populations. The situation of the methyl group on the benzamide ring of the SDHI can also affect the biological activity of the fungicides. Actually, various mergings of strobilurins by SDHI compounds through a dual combination (Table 5) with an additional aromatic ring between the two active moieties exhibited high activity. Interestingly, the activity decreased with the increase in the chain length. Changing the aromatic ring in the SDHI moiety by replacing the benzamide with a heterocyclic amide maintained good activity of the dual compounds against WT strains (Tables 5, 6). Moreover, changing the aromaticity due to climate changes in climate, such as temperature, wetness, pressure, and pH of the soil, as well as greenhouse gases and global warming, causes changes in the NICS index; a new dual combination will be changed based on this new climate. Finally, the changing parameters of global warming, temperature change, and forest wetness, and the subsequent changes in the various modes of action of SDHI compounds through dual combinations, lead us to synthesize novel pesticides and microbial bio-fungicides based on the new climate parameters, as shown in Table 7. Despite the promising docking and structural results, this study has several limitations. The proposed SDHI–QoI hybrid fungicides were evaluated primarily through computational modeling, without experimental validation of antifungal activity. In addition, synthetic feasibility, physicochemical properties (e.g., solubility, lipophilicity, and stability), and ADMET-related parameters were not assessed. These factors are critical for determining practical applicability, environmental safety, and regulatory suitability. Future work should include synthesis, in vitro and in vivo bioassays, and comprehensive physicochemical and ecotoxicological evaluation. In addition, while NICS values provide a measure of Aromaticity and electronic stability for the designed dual SDHI–QoI fungicides, they are intrinsic molecular properties and are not directly influenced by environmental factors. However, climate variables such as temperature, soil pH, moisture, and humidity can affect the stability, solubility, bioavailability, and overall efficacy of fungicides in agricultural settings. Therefore, in designing climate-adaptive fungicides, NICS and structural descriptors can guide the intrinsic potency of the molecules, while additional modeling or experimental studies are needed to account for environmental conditions that impact their field performance. By integrating molecular design with climate-dependent factors that affect fungicide behavior, it is possible to optimize dual-action compounds for robust activity across diverse environmental conditions.

Table 7. Phytopathogens for host fruits and vegetables due to disease and biocontrol agents.

Phytopathogen	Hosts	Diseases	Biocontrol agents	References
Botrytis cinerea	Apple	Gray mold	*Metschnikowia pulcherrima*	[102]
Botrytis cinerea and *Penicillium italicum*	Apple	Blue mold	*Pichia membranifaciens*and*Wickerhamomyces anomalus*	[103]
Botrytis cinerea	Grapes	Gray mold	*Meyerozyma guilliermondii* and *Aureobasidium pullulans*	[104]
Botrytis cinerea and *Penicillium expansum*	Apple	Apple rot	*Aureobasidium subglaciale*	[105]
Colletotrichum gloeosporioides	Avocado	Anthracnose	*Yamadazyma mexicana*	[106]
Penicillium digitatum	Citrus	Green mold	*Lactobacillus plantarum and Lactobacillus plantarum*	[107]
Penicillium digitatum	Mandarin fruits	Green mold	*Metschnikowia pulcherrima*, *Pichia guilliermondii*	[108]
Penicillium digitatum	Citrus	Green mold	*Pichia kudriavzevii*	[109]
Fusarium solani and Fusarium oxysporum	Dry bean	Wiltdiseases	*Trichoderma*spp.	[110]
Botrytis cinerea	Grapes	Gray mold	*Bacillus amyloliquefaciens*	[111]
Pestalotiopsis theae	Tea plants	Gray blight	Paecilomyces lilacinus	[112]
Plasmodiophora brassicae	Pak choi	Clubroot	Clubroot	[113]
Colletotrichum gloeosporioides	Mango	Anthracnose	*Penicillium citrinum*	[114]
Penicillium digitatum and *Penicillium italicum*	Orange	Green mold and blue	*Bacillus amyloliquefaciens*, *Bacillus pumilus*, and*Bacillus*	[115]
Geotrichum citri-aurantii	Lemon	Green mold	*Bacillus amyloliquefaciens*, *Bacillus pumilus*, and*Bacillus*	[115]
Aspergillus favus	Rice	Rice mold	*Bacillus velezensis*	[116]
Colletotrichum gloeosporioides	Chili pepper	Anthracnose	*Trichoderma koningiopsis*	[117]
Fusarium oxysporum	Potato	Fusarium rot	*Bacillus*sp.	[118]
Aspergillus favus	Tomato	Spoilage	*Aureobasidium pullulans*	[119]
Botrytis cinerea	Strawberry	Gray mold	*Lactobacillus plantarum*	[120]
Lactobacillus plantarum	Vineyard	Gray mold	*Metschnikowia pulcherrima*and*Aureobasidium pullulans*	[121]

4. Conclusions

The effectiveness of fungicides is gradually decreasing due to climate change, global warming, and modernization of agricultural practices, highlighting the growing threat of fungicide-resistant pathogens to human life and food security. Understanding the mechanisms of QoI fungicide resistance is critical for designing more potent inhibitors that control plant diseases without damaging forests, rivers, or ecological systems. In this study, we merged various SDHI and strobilurin (QoI) fungicides into hybrid dual-action molecules. The methoxy acrylate groups of strobilurins interacted with residues F129L and G137R of the C-helix, while hydrogen bonds, π–π stacking, and van der Waals interactions contributed to binding at the Qo-active site. Docking simulations showed that these dual-action molecules exhibited more

favorable binding energies (i.e., more negative ΔG) than several commercial fungicides, indicating greater inhibitory potential. The presence of aromatic benzene rings in both SDHI and strobilurin moieties stabilizes the hybrid compounds through π–π stacking interactions. We observed that placing the SDHI and QoI pharmacophores in an ortho configuration on the central ring maximized activity against wild-type fungal strains. The aromaticity of central rings was quantified using nucleus-independent chemical shift (NICS) calculations, which provide a measure of electronic delocalization and current density and indirectly reflect electronic stability. Modifications of the SDHI moiety, such as replacing benzamide with a heterocyclic amide, maintained good activity while influencing aromaticity patterns. A linear relationship between NICS-derived aromaticity and predicted pesticidal activity was established, enabling rational design of dual fungicides. Although NICS is an intrinsic molecular property, integrating docking results with climatic factors such as temperature, soil pH, moisture, and greenhouse gas levels enables climate-adaptive simulation of fungicide efficacy. This approach provides a framework for designing novel hybrid SDHI-strobilurin fungicides and microbial bio-fungicides tailored for various fruit, vegetable, and forestry climates, accounting for environmental and ecological parameters.

Author Contributions

Conceptualization, MM and TÇ; methodology, MM; software, FM; validation, MM, OB, TÇ and FM; investigation, MM and TÇ; resources, FM and OB; data curation, MM, OB, TÇ and FM; writing—original draft preparation, MM and FM; writing—review and editing, MM and TÇ; visualization, FM and OB; supervision, MM; project administration, MM. All authors have read and agreed to the published version of the manuscript.

Institutional Review Board Statement

Not applicable.

Informed Consent Statement

Not applicable.

Data Availability Statement

Not applicable.

Funding

This research received no external funding.

Acknowledgments

The authors are grateful to Kastamonu University for successfully completing this paper and its research.

Conflict of Interest

The authors declare no conflict of interest.

References

1. Andersen, K.L.; Sebolt, A.M.; Sundin, G.W.; Iezzoni, A.F. Assessment of the inheritance of resistance and tolerance in cherry (*Prunus* sp.) to *Blumeriella jaapii*, the causal agent of cherry leaf spot. *Plant Pathology* **2018**, *67*, 682-691, https://doi.org/10.1111/ppa.12765.
2. Proffer, T.J.; Berardi, R.; Ma, Z.; Nugent, J.E.; Ehret, G.R.; McManus, P.S.; Jones, A.L.; Sundin, G.W. Occurrence, Distribution, and Polymerase Chain Reaction-Based Detection of Resistance to Sterol Demethylation Inhibitor Fungicides in Populations of *Blumeriella jaapii* in Michigan. *Phytopathology®* **2006**, *96*, 709-717, https://doi.org/10.1094/PHYTO-96-0709.
3. Ma, Z.; Proffer Tyre, J.; Jacobs Janette, L.; Sundin George, W. Overexpression of the 14α-Demethylase Target Gene (*CYP51*) Mediates Fungicide Resistance in *Blumeriella jaapii*. *Appl. Environ. Microbiol.* **2006**, *72*, 2581-2585, https://doi.org/10.1128/AEM.72.4.2581-2585.2006.
4. Kamp, H.; Wahrheit, J.; Stinchcombe, S.; Walk, T.; Stauber, F.; Ravenzwaay, B.v. Succinate dehydrogenase inhibitors: *in silico* flux analysis and *in vivo* metabolomics investigations show no severe metabolic consequences for rats and humans. *Food Chem. Toxicol.* **2021**, *150*, 112085, https://doi.org/10.1016/j.fct.2021.112085.
5. Outwater, C.A.; Proffer, T.J.; Rothwell, N.L.; Peng, J.; Sundin, G.W. Boscalid Resistance in *Blumeriella jaapii*: Distribution, Effect on Field Efficacy, and Molecular Characterization. *Plant Dis.* **2019**, *103*, 1112-1118, https://doi.org/10.1094/PDIS-09-18-1555-RE.
6. Avenot, H.F.; Michailides, T.J. Progress in understanding molecular mechanisms and evolution of resistance to succinate dehydrogenase inhibiting (SDHI) fungicides in phytopathogenic fungi. *Crop Prot.* **2010**, *29*, 643–651, https://doi.org/10.1016/j.cropro.2010.02.019.
7. Heaney, S.P.; Hall, A.A.; Davies, S.A.; Olaya, G. Resistance to fungicides in the Qol-STAR cross-resistance group: Current perspectives. In Proceedings of the BCPC Conference: Pests and Diseases, Brighton, UK, 13–16 November 2000; Volume 2, pp. 755–762.
8. Mallik, I.; Arabiat, S.; Pasche, J.S.; Bolton, M.D.; Patel, J.S.; Gudmestad, N.C. Molecular Characterization and Detection of Mutations Associated with Resistance to Succinate Dehydrogenase-Inhibiting Fungicides in *Alternaria solani*. *Phytopathology®* **2013**, *104*, 40-49, https://doi.org/10.1094/PHYTO-02-13-0041-R.
9. Grabau, Z.J.; Liu, C.; Schumacher, L.A.; Small, I.M.; Wright, D.L. In-furrow fluopyram nematicide efficacy for *Rotylenchulus reniformis* management in cotton production. *Crop Prot.* **2021**, *140*, 105423, https://doi.org/10.1016/j.cropro.2020.105423.
10. Cecchini, G. Function and Structure of Complex II of the Respiratory Chain. *Annu. Rev. Biochem.* **2003**, *72*, 77–109, https://doi.org/10.1146/annurev.biochem.72.121801.161700.
11. Avenot, H.F.; Thomas, A.; Gitaitis, R.D.; Langston Jr, D.B.; Stevenson, K.L. Molecular characterization of boscalid- and penthiopyrad-resistant isolates of *Didymella bryoniae* and assessment of their sensitivity to fluopyram. *Pest Manag. Sci.* **2012**, *68*, 645-651, https://doi.org/10.1002/ps.2311.
12. Veloukas, T.; Markoglou, A.N.; Karaoglanidis, G.S. Differential Effect of *SdhB* Gene Mutations on the Sensitivity to SDHI Fungicides in *Botrytis cinerea*. *Plant Dis.* **2012**, *97*, 118-122, https://doi.org/10.1094/PDIS-03-12-0322-RE.
13. Amiri, A.; Heath, S.M.; Peres, N.A. Resistance to Fluopyram, Fluxapyroxad, and Penthiopyrad in *Botrytis cinerea* from Strawberry. *Plant Dis.* **2013**, *98*, 532-539, https://doi.org/10.1094/PDIS-07-13-0753-RE.
14. Yang, J.H.; Brannen, P.M.; Schnabel, G. Resistance in *Alternaria alternata* to SDHI Fungicides Causes Rare Disease Outbreak in Peach Orchards. *Plant Dis.* **2014**, *99*, 65-70, https://doi.org/10.1094/PDIS-04-14-0387-RE.
15. Hu, M.-J.; Fernández-Ortuño, D.; Schnabel, G. Monitoring Resistance to SDHI Fungicides in *Botrytis cinerea* From Strawberry Fields. *Plant Dis.* **2015**, *100*, 959-965, https://doi.org/10.1094/PDIS-10-15-1210-RE.
16. Fernández-Ortuño, D.; Pérez-García, A.; Chamorro, M.; de la Peña, E.; de Vicente, A.; Torés, J.A. Resistance to the SDHI Fungicides Boscalid, Fluopyram, Fluxapyroxad, and Penthiopyrad in *Botrytis cinerea* from Commercial Strawberry Fields in Spain. *Plant Dis.* **2017**, *101*, 1306-1313, https://doi.org/10.1094/PDIS-01-17-0067-RE.

17. Popko, J.T.; Sang, H.; Lee, J.; Yamada, T.; Hoshino, Y.; Jung, G. Resistance of *Sclerotinia homoeocarpa* Field Isolates to Succinate Dehydrogenase Inhibitor Fungicides. *Plant Dis.* **2018**, *102*, 2625-2631, https://doi.org/10.1094/PDIS-12-17-2025-RE.
18. Lee, J.; Elliott, M.R.; Yamada, T.; Jung, G. Field Assessment of Six Point-Mutations in SDH Subunit Genes Conferring Varying Resistance Levels to SDHIs in *Clarireedia* spp. *Plant Dis.* **2021**, *105*, 1685-1691, https://doi.org/10.1094/PDIS-06-20-1344-RE.
19. Strathmann, S.; Walker, S.; Barnes, J. Fluxapyroxad: A new broad-spectrum fungicide. *Phytopathology* **2011**, *101*,172.
20. Li, H.-X.; Nuckols, T.A.; Harris, D.; Stevenson, K.L.; Brewer, M.T. Differences in fungicide resistance profiles and multiple resistance to a quinone-outside inhibitor (QoI), two succinate dehydrogenase inhibitors (SDHI), and a demethylation inhibitor (DMI) for two *Stagonosporopsis* species causing gummy stem blight of cucurbits. *Pest Manag. Sci.* **2019**, *75*, 3093-3101, https://doi.org/10.1002/ps.5426.
21. Shi, Y.; Zhu, F.; Sun, B.; Xie, X.; Chai, A.; Li, B. Two adjacent mutations in the conserved domain of SdhB confer various resistance phenotypes to fluopyram in *Corynespora cassiicola*. *Pest Manag. Sci.* **2021**, *77*, 3980-3989, https://doi.org/10.1002/ps.6420.
22. Ma, Z.; Proffer, T.J.; Jacobs, J.L.; Sundin, G.W. Overexpression of the 14α-demethylase target gene (*CYP51*) mediates fungicide resistance in *Blumeriella jaapii*. *Appl. Environ. Microbiol.* **2006**, *72*, 2581–2585. doi: 10.1128/AEM.72.4.2581-2585.2006
23. Peng, J.; Sang, H.; Proffer, T.J.; Gleason, J.; Outwater, C.A.; Jung, G.; Sundin, G.W. A Method for the Examination of SDHI Fungicide Resistance Mechanisms in Phytopathogenic Fungi Using a Heterologous Expression System in Sclerotinia sclerotiorum. *Phytopathology®* **2020**, *111*, 819-830, https://doi.org/10.1094/PHYTO-09-20-0421-R.
24. Mollaamin, F. Computational Methods in the Drug Delivery of Carbon Nanocarriers onto Several Compounds in Sarraceniaceae Medicinal Plant as Monkeypox Therapy. *Computation* **2023**, *11*, 84, https://doi.org/10.3390/computation11040084.
25. Gadoury, D.M.; Cadle-Davidson, L.; Wilcox, W.F.; Dry, I.B.; Seem, R.C.; Milgroom, M.G. Grapevine powdery mildew (*Erysiphe necator*): a fascinating system for the study of the biology, ecology and epidemiology of an obligate biotroph. *Mol. Plant Pathol.* **2012**, *13*, 1-16, https://doi.org/10.1111/j.1364-3703.2011.00728.x.
26. Calonnec, A.; Cartolaro, P.; Poupot, C.; Dubourdieu, D.; Darriet, P. Effects of *Uncinula necator* on the yield and quality of grapes (*Vitis vinifera*) and wine. *Plant Pathol.* **2004**, *53*, 434-445, https://doi.org/10.1111/j.0032-0862.2004.01016.x.
27. Gadoury, D.M.; Seem, R.C.; Ficke, A.; Wilcox, W.F. The Epidemiology of Powdery Mildew on Concord Grapes. *Phytopathology®* **2001**, *91*, 948-955, https://doi.org/10.1094/phyto.2001.91.10.948.
28. Jones, L.; Riaz, S.; Morales-Cruz, A.; Amrine, K.C.H.; McGuire, B.; Gubler, W.D.; Walker, M.A.; Cantu, D. Adaptive genomic structural variation in the grape powdery mildew pathogen, *Erysiphe necator*. *BMC Genomics* **2014**, *15*, 1081, https://doi.org/10.1186/1471-2164-15-1081.
29. Rantsiou, K.; Giacosa, S.; Pugliese, M.; Englezos, V.; Ferrocino, I.; Río Segade, S.; Monchiero, M.; Gribaudo, I.; Gambino, G.; Gullino, M.L.; Rolle, L. Impact of Chemical and Alternative Fungicides Applied to Grapevine cv Nebbiolo on Microbial Ecology and Chemical-Physical Grape Characteristics at Harvest. *Front. Plant Sci.* **2020**, *11*, 700, https://doi.org/10.3389/fpls.2020.00700.
30. Stummer, B.E.; Francis, I.L.; Markides, A.J.; Scott, E.S. The effect of powdery mildew infection of grape berries on juice and wine composition and on sensory properties of Chardonnay wines. *Aust. J. Grape Wine Res.* **2003**, *9*, 28-39, https://doi.org/10.1111/j.1755-0238.2003.tb00229.x.
31. Gaforio, L.; García-Muñoz, S.; Cabello, F.; Muñoz-Organero, G. Evaluation of susceptibility to powdery mildew (*Erysiphe necator*) in *Vitis vinifera* varieties. *Vitis - J. Grapevine Res.* **2015**, *50*, 123, https://doi.org/10.5073/vitis.2011.50.123-126.
32. Staudt, G. Evaluation of resistance to grapevine powdery mildew (*Uncinula necator* [Schw.] Burr., anamorph *Oidium tuckeri* Berk.) in accessions of *Vitis* species. *Vitis* **2015**, *36*, 151, https://doi.org/10.5073/vitis.1997.36.151-154.
33. Dry, I.B.; Feechan, A.; Anderson, C.; Jermakow, A.M.; Bouquet, A.; Adam-Blondon, A.F.; Thomas, M.R. Molecular strategies to enhance the genetic resistance of grapevines to powdery mildew. *Aust. J. Grape Wine Res.* **2010**, *16*, 94-105, https://doi.org/10.1111/j.1755-0238.2009.00076.x.

34. Gianessi, L.; Williams, A. Fungicides have protected European wine grapes for 150 years. *Int. Pestic. Benefits Case Study* **2011**, *19*.
35. Savas, N.G.; Akgul, D.S.; Albaz, E.; Savas, Y.; Onder, S. ASSESSMENT OF A FORECAST-WARNING MODEL FOR THE CONTROL OF GRAPEVINE POWDERY MILDEW IN THE AEGEAN REGION IN TURKEY. *Fresenius Environ. Bull.* **2022**, *31*, 2840-2849.
36. *Fungicide Resistance Action Committee (FRAC).* FRAC Code List© 2024: Fungal Control Agents Sorted by Cross-Resistance Pattern and Mode of Action (Including Coding for FRAC Groups on Product Labels)*; FRAC: Frankfurt, Germany, 2024.*
37. Vielba-Fernández, A.; Polonio, Á.; Ruiz-Jiménez, L.; de Vicente, A.; Pérez-García, A.; Fernández-Ortuño, D. Fungicide Resistance in Powdery Mildew Fungi. *Microorganisms* **2020**, *8*, 1431, https://doi.org/10.3390/microorganisms8091431.
38. Morton, V.; Staub, T. A Short History of Fungicides. *APSnet Feature* **2008**, *308*, 1–5.
39. Klittich, C.J. Milestones in Fungicide Discovery: Chemistry that Changed Agriculture. *Plant Health Prog.* **2008**, *9*, 31, https://doi.org/10.1094/PHP-2008-0418-01-RV.
40. Davidse, L.C. Antimitotic activity of methyl benzimidazol-2-yl carbamate (MBC) in *Aspergillus nidulans*. *Pestic. Biochem. Physiol.* **1973**, *3*, 317–325, https://doi.org/10.1016/0048-3575(73)90030-8.
41. Pearson, R.C.; Taschenberg, E.F. Benomyl-Resistant Strains of *Uncinula necator* on Grapes. *Plant Dis.* **1980**, *64*, 677–680.
42. Vela-Corcía, D.; Romero, D.; de Vicente, A.; Pérez-García, A. Analysis of β-tubulin-carbendazim interaction reveals that binding site for MBC fungicides does not include residues involved in fungicide resistance. *Sci. Rep.* **2018**, *8*, 7161, https://doi.org/10.1038/s41598-018-25336-5.
43. Opalski, K. Cell polarity in plant defense and fungal pathogenesis in the interaction of barley with powdery mildew fungi. Doctoral Thesis, Justus-Liebig-University Giessen, Germany, **2005**.
44. Schmitt, M.R.; Carzaniga, R.; Cotter, H.V.T.; O'Connell, R.; Hollomon, D. Microscopy reveals disease control through novel effects on fungal development: a case study with an early-generation benzophenone fungicide. *Pest Manag. Sci.* **2006**, *62*, 383-392, https://doi.org/10.1002/ps.1177.
45. Kunova, A.; Pizzatti, C.; Bonaldi, M.; Cortesi, P. Metrafenone resistance in a population of *Erysiphe necator* in northern Italy. *Pest Manag. Sci.* **2016**, *72*, 398–404, https://doi.org/10.1002/ps.4060.
46. Naegler, M.; Diaconu, V.; Alexandri, A.A. The resistance of powdery mildew of vine (*Uncinula necator*) and powdery mildew of cucumber (*Sphaerotheca fuliginea*) to benzimidazole systemic fungicides. *An. Inst. Cercet. Pentru Prot. Plantelor* **1977**, *12*, 345–352.
47. Cherrad, S.; Charnay, A.; Hernandez, C.; Steva, H.; Belbahri, L.; Vacher, S. Emergence of boscalid-resistant strains of *Erysiphe necator* in French vineyards. *Microbiol. Res.* **2018**, *216*, 79–84, https://doi.org/10.1016/j.micres.2018.08.007.
48. Miller, T.C.; Gubler, W.D. Sensitivity of California isolates of *Uncinula necator* to trifloxystrobin and spiroxamine, and update on triadimefon sensitivity. *Plant Dis.* **2004**, *88*, 1205–1212, https://doi.org/10.1094/PDIS.2004.88.11.1205.
49. Genet, J.-L.; Jaworska, G. Baseline sensitivity to proquinazid in *Blumeria graminis* f. sp. *tritici* and *Erysiphe necator* and cross-resistance with other fungicides. *Pest Manag. Sci.* **2009**, *65*, 878–884, https://doi.org/10.1002/ps.1768.
50. Steva, H.; Cartolaro, P.; Silva, M. Tolerance of powdery mildew of SBI fungicides: Situation for 1989. *Phytoma* **1990**, *419*, 41–44.
51. Gubler, W.D.; Ypema, H.L.; Ouimette, D.G.; Bettiga, L.J. Occurrence of resistance in *Uncinula necator* to triadimefon, myclobutanil, and fenarimol in California grapevines. *Plant Dis.* **1996**, *80*, 902–909, https://doi.org/10.1094/PD-80-0902.
52. Halleen, F.; Holz, G.; Pringle, K.L. Resistance in *Uncinula necator* to triazole fungicides in South African grapevines. *South Afr. J. Enol. Vitic.* **2000**, *21*, 71–80, https://doi.org/10.21548/21-2-2213.
53. Mollaamin, F. PHYSICOCHEMICAL INVESTIGATION OF ANTI-COVID19 DRUGS USING SEVERAL MEDICINAL PLANTS. *J. Chil. Chem. Soc.* **2022**, 67, 5537–5546, https://doi.org/10.4067/S0717-97072022000205537.
54. Balba, H. Review of strobilurin fungicide chemicals. *J. Environ. Sci. Health Part B* **2007**, *42*, 441–451, https://doi.org/10.1080/03601230701316465.
55. Bartlett, D.W.; Clough, J.M.; Godwin, J.R.; Hall, A.A.; Hamer, M.; Parr-Dobrzanski, B. The strobilurin fungicides. *Pest Manag. Sci.* **2002**, *58*, 649–662, https://doi.org/10.1002/ps.520.

56. Rodrigues, E.T.; Lopes, I.; Pardal, M.Â. Occurrence, fate and effects of azoxystrobin in aquatic ecosystems: A review. *Environ. Int.* **2013**, *53*, 18-28, https://doi.org/10.1016/j.envint.2012.12.005.
57. Mollaamin, F. Structural and Functional Characterization of Medicinal Plants as Selective Antibodies towards Therapy of COVID-19 Symptoms. *Antibodies* **2024**, *13*, 38, https://doi.org/10.3390/antib13020038.
58. Sauter, H.; Steglich, W.; Anke, T. Strobilurins: Evolution of a New Class of Active Substances. *Angew. Chem. Int. Ed.* **1999**, *38*, 1328–1349, https://doi.org/10.1002/(sici)1521-3773(19990517)38:10%3C1328::aid-anie1328%3E3.0.co;2-1.
59. Papadopoulos, J.S.; Agarwala, R. COBALT: constraint-based alignment tool for multiple protein sequences. *Bioinformatics* **2007**, *23*, 1073–1079, https://doi.org/10.1093/bioinformatics/btm076.
60. Sierotzki, H.; Scalliet, G. A Review of Current Knowledge of Resistance Aspects for the Next-Generation Succinate Dehydrogenase Inhibitor Fungicides. *Phytopathology* **2013**, *103*, 880–887, https://doi.org/10.1094/PHYTO-01-13-0009-RVW.
61. Hunte, C.; Koepke, J.; Lange, C.; Roßmanith, T.; Michel, H. Structure at 2.3 Å resolution of the cytochrome bc1 complex from the yeast *Saccharomyces cerevisiae* co-crystallized with an antibody Fv fragment. *Structure* **2000**, *8*, 669-684, https://doi.org/10.1016/S0969-2126(00)00152-0.
62. Fisher, N.; Meunier, B. Re-examination of inhibitor resistance conferred by Q_o-site mutations in cytochrome b using yeast as a model system. *Pest Manag. Sci*. **2005**, *61*, 973–978, https://doi.org/10.1002/ps.1066.
63. Suemoto, H.; Matsuzaki, Y.; Iwahashi, F. Metyltetraprole, a novel putative complex III inhibitor, targets known QoI-resistant strains of *Zymoseptoria tritici* and *Pyrenophora teres*. *Pest Manag. Sci.* **2019**, *75*, 1181-1189, https://doi.org/10.1002/ps.5288.
64. Harder, E.; Damm, W.; Maple, J.; Wu, C.; Reboul, M.; Xiang, J.Y.; Wang, L.; Lupyan, D.; Dahlgren, M.K.; Knight, J.L.; Kaus, J.W.; Cerutti, D.S.; Krilov, G.; Jorgensen, W.L.; Abel, R.; Friesner, R.A. OPLS3: A Force Field Providing Broad Coverage of Drug-like Small Molecules and Proteins. *J. Chem. Theory Comput.* **2016**, *12*, 281-296, https://doi.org/10.1021/acs.jctc.5b00864.
65. Esser, L.; Quinn, B.; Li, Y.-F.; Zhang, M.; Elberry, M.; Yu, L.; Yu, C.-A.; Xia, D. Crystallographic Studies of Quinol Oxidation Site Inhibitors: A Modified Classification of Inhibitors for the Cytochrome bc_1 Complex. *J. Mol. Biol.* **2004**, *341*, 281-302, https://doi.org/10.1016/j.jmb.2004.05.065.
66. Friesner, R.A.; Banks, J.L.; Murphy, R.B.; Halgren, T.A.; Klicic, J.J.; Mainz, D.T.; Repasky, M.P.; Knoll, E.H.; Shelley, M.; Perry, J.K.; Shaw, D.E.; Francis, P.; Shenkin, P.S. Glide: A New Approach for Rapid, Accurate Docking and Scoring. 1. Method and Assessment of Docking Accuracy. *J. Med. Chem.* **2004**, *47*, 1739-1749, https://doi.org/10.1021/jm0306430.
67. Halgren, T.A.; Murphy, R.B.; Friesner, R.A.; Beard, H.S.; Frye, L.L.; Pollard, W.T.; Banks, J.L. Glide: A New Approach for Rapid, Accurate Docking and Scoring. 2. Enrichment Factors in Database Screening. *J. Med. Chem.* **2004**, *47*, 1750-1759, https://doi.org/10.1021/jm030644s.
68. Friesner, R.A.; Murphy, R.B.; Repasky, M.P.; Frye, L.L.; Greenwood, J.R.; Halgren, T.A.; Sanschagrin, P.C.; Mainz, D.T. Extra Precision Glide: Docking and Scoring Incorporating a Model of Hydrophobic Enclosure for Protein−Ligand Complexes. *J. Med. Chem.* **2006**, *49*, 6177-6196, https://doi.org/10.1021/jm051256o.
69. Li, J.; Abel, R.; Zhu, K.; Cao, Y.; Zhao, S.; Friesner, R.A. The VSGB 2.0 model: A next generation energy model for high resolution protein structure modeling. *Proteins: Struct. Funct. Bioinform.* **2011**, *79*, 2794-2812, https://doi.org/10.1002/prot.23106.
70. Eberini, I.; Rocco, A.G.; Mantegazza, M.; Gianazza, E.; Baroni, A.; Vilardo, M.C.; Donghi, D.; Galliano, M.; Beringhelli, T. Computational and experimental approaches assess the interactions between bovine β-lactoglobulin and synthetic compounds of pharmacological interest. *J. Mol. Graph. Model.* **2008**, *26*, 1004-1013, https://doi.org/10.1016/J.JMGM.2007.08.006.
71. Sun, B.; Zhu, G.; Xie, X.; Chai, A.; Li, L.; Shi, Y.; Li, B. Double Mutations in Succinate Dehydrogenase Are Involved in SDHI Resistance in *Corynespora cassiicola*. *Microorganisms* **2022**, *10*, 132, https://doi.org/10.3390/microorganisms10010132.
72. Monajjemi, M. Quantum investigation of non-bonded interaction between the $B_{15}N_{15}$ ring and BH_2NBH_2 (radical, cation, anion) systems: a nano molecularmotor. *Struct. Chem.* **2012**, *23*, 551–580, https://doi.org/10.1007/s11224-011-9895-8.

73. Monajjemi, M.; Ketabi, S.; Amiri, A. Monte Carlo simulation study of melittin: Protein folding and temperature dependence. *Russ. J. Phys. Chem.* **2006**, *80*, S55-S62, https://doi.org/10.1134/S0036024406130103.
74. Monajjemi, M. Metal-doped graphene layers composed with boron nitride–graphene as an insulator: a nano-capacitor. *J. Mol. Model.* **2014**, *20*, 2507, https://doi.org/10.1007/s00894-014-2507-y.
75. Monajjemi, M.; Boggs, J.E. A New Generation of B_nN_n Rings as a Supplement to Boron Nitride Tubes and Cages. *J. Phys. Chem. A* **2013**, *117*, 1670-1684, https://doi.org/10.1021/jp312073q.
76. Monajjemi, M.; Heshmata, M.; Haeria, H.H. QM/MM model study on properties and structure of some antibiotics in gas phase: Comparison of energy and NMR chemical shift. *Biochemistry* **2006**, *71*, S113-S122, https://doi.org/10.1134/S0006297906130190.
77. Monajjemi, M. Non bonded interaction between B_nN_n (stator) and $BN(^{-,0,+})B$ (rotor) systems: A quantum rotation in IR region. *Chem. Phys.* **2013**, *425*, 29-45, https://doi.org/10.1016/j.chemphys.2013.07.014.
78. Monajjemi, M. Cell membrane causes the lipid bilayers to behave as variable capacitors: A resonance with self-induction of helical proteins. *Biophys. Chem.* **2015**, *207*, 114-127, https://doi.org/10.1016/j.bpc.2015.10.003.
79. Mollaamin, F.; Monajjemi, M. DFT outlook of solvent effect on function of nano bioorganic drugs. *Phys. Chem. Liq.* **2012**, *50*, 596-604, https://doi.org/10.1080/00319104.2011.646444.
80. Mahdavian, L.; Monajjemi, M.; Mangkorntong, N. Sensor Response to Alcohol and Chemical Mechanism of Carbon Nanotube Gas Sensors. *Fuller. Nanotub. Carbon Nanostruct.* **2009**, *17*, 484-495, https://doi.org/10.1080/15363830903130044.
81. Monajjemi, M. Liquid-phase exfoliation (LPE) of graphite towards graphene: An ab initio study. *J. Mol. Liq.* **2017**, *230*, 461–472, https://doi.org/10.1016/j.molliq.2017.01.044.
82. Monajjemi, M.; Mahdavian, L.; Mollaamin, F. Characterization of nanocrystalline silicon germanium film and nanotube in adsorption gas by Monte Carlo and Langevin dynamic simulation. *Bull. Chem. Soc. Ethiop.* **2008**, *22*, 277-286, https://doi.org/10.4314/bcse.v22i2.61299.
83. Monajjemi, M.; Wayne, R.; Boggs, J.E. NMR contour maps as a new parameter of carboxyl's OH groups in amino acids recognition: A reason of tRNA–amino acid conjugation. *Chem. Phys.* **2014**, *433*, 1-11, https://doi.org/10.1016/j.chemphys.2014.01.017.
84. Jalilian, H.; Monajjemi, M. Capacitor simulation including of X-doped graphene (X = Li, Be, B) as two electrodes and $(h\text{-}BN)_m$ (m = 1–4) as the insulator. *Jpn. J. Appl. Phys.* **2015**, *54*, 085101, https://doi.org/10.7567/JJAP.54.085101.
85. Monajjemi, M. Non-covalent attraction of $B_2N^{(-,0)}$ and repulsion of $B_2N^{(+)}$ in the B_nN_n ring: a quantum rotatory due to an external field. *Theor. Chem. Acc.* **2015**, *134*, 77, https://doi.org/10.1007/s00214-015-1668-9.
86. Monajjemi, M.; Naderi, F.; Mollaamin, F.; Khaleghian, M. Drug Design Outlook by Calculation of Second Virial Coefficient as a Nano Study. *J. Mex. Chem. Soc.* **2012**, *56*, 207-211, https://doi.org/10.29356/jmcs.v56i2.323.
87. Monajjemi, M.; Bagheri, S.; Moosavi, M.S.; Moradiyeh, N.; Zakeri, M.; Attarikhasraghi, N.; Saghayimarouf, N.; Niyatzadeh, G.; Shekarkhand, M.; Khalilimofrad, M.S.; *et al*. Symmetry Breaking of $B_2N^{(-,\,0,\,+)}$: An Aspect of the Electric Potential and Atomic Charges. *Molecules* **2015**, *20*, 21636-21657. https://doi.org/10.3390/molecules201219769.
88. Monajjemi, M.; Mahdavian, L.; Mollaamin, F.; Honarparvar, B. Thermodynamic Investigation of Enol↔Keto Tautomerism for Alcohol Sensors Based on Carbon Nanotubes as Chemical Sensors. *Fuller. Nanotub. Carbon Nanostruct.* **2010**, *18*, 45-55, https://doi.org/10.1080/15363830903291564.
89. Monajjemi, M.; Ketabi, S.; Hashemian Zadeh, M.; Amiri, A. Simulation of DNA bases in water: Comparison of the Monte Carlo algorithm with molecular mechanics force fields. *Biochemistry* **2006**, *71*, S1-S8, https://doi.org/10.1134/s0006297906130013.
90. Ilkhani, A.R.; Monajjemi, M. The pseudo Jahn–Teller effect of puckering in pentatomic unsaturated rings C_4AE_5, A=N, P, As, E=H, F, Cl. *Comput. Theor. Chem.* **2015**, *1074*, 19-25, https://doi.org/10.1016/j.comptc.2015.10.006.
91. Mollaamin, F.; Najafpour, J.; Ghadami, S.; Ilkhani, A.R.; Akrami, M.S.; Monajjemi, M. The Electromagnetic Feature of $B_{15}N_{15}H_x$ (x= 0, 4, 8, 12, 16, and 20) Nano Rings: Quantum Theory of Atoms in Molecules/NMR Approach. *J. Comput. Theor. Nanosci.* **2014**, *11*, 1290-1298.

92. Monajjemi, M.; Lee, V.S.; Khaleghian, M.; Honarparvar, B.; Mollaamin, F. Theoretical Description of Electromagnetic Nonbonded Interactions of Radical, Cationic, and Anionic $NH_2BHNBHNH_2$ Inside of the $B_{18}N_{18}$ Nanoring. *J. Phys. Chem. C* **2010**, *114*, 15315-15330, https://doi.org/10.1021/jp104274z.
93. Mollaamin, F.; Monajjemi, M. Fractal dimension on carbon nanotube-polymer composite materials using percolation theory. *J. Comput. Theor. Nanosci.* **2012**, *9*, 597-601, https://doi.org/10.1166/jctn.2012.2067.
94. Zhang, Z.; Zheng, M.; Du, L.; Shen, J.; Luo, X.; Zhu, W.; Jiang, H. Towards discovering dual functional inhibitors against both wild type and K103N mutant HIV-1 reverse transcriptases: molecular docking and QSAR studies on 4,1-benzoxazepinone analogues. *J. Comput.-Aided Mol. Des.* **2006**, *20*, 281-293, https://doi.org/10.1007/s10822-006-9050-6.
95. Bühl, M.; van Wüllen, C. Computational evidence for a new C_{84} isomer. *Chem. Phys. Lett.* **1995**, *247*, 63-68, https://doi.org/10.1016/0009-2614(95)01193-6.
96. Schleyer, P.v.R.; Maerker, C.; Dransfeld, A.; Jiao, H.; van Eikema Hommes, N.J.R. Nucleus-Independent Chemical Shifts: A Simple and Efficient Aromaticity Probe. *J. Am. Chem. Soc.* **1996**, *118*, 6317-6318, https://doi.org/10.1021/ja960582d.
97. Haeberlen, U. High Resolution NMR in Solids. *Advances in Magnetic Resonance Academic Press, New York* **1976**.
98. Mehring, M. Principles of High Resolution NMR in Solids; Springer Berlin Heidelberg: Berlin, Heidelberg, **1983**; https://doi.org/10.1007/978-3-642-68756-3.
99. Diehl, P.; Fluck, E.; Kosfeld, R. *Van der Waals Forces and Shielding Effects*; Springer-Verlag: Berlin/Heidelberg, Germany, 1975; Part of the series *NMR Basic Principles and Progress*; Volume 10. https://doi.org/10.1007/978-3-642-66176-1.
100. Harris, R.K.; Becker, E.D.; De Menezes, S.M.C.; Granger, P.; Hoffman, R.E.; Zilm, K.W. Further Conventions for NMR Shielding and Chemical Shifts (IUPAC Recommendations 2008). *Magn. Reson. Chem.* **2008**, *46*, 582-598, https://doi.org/10.1002/mrc.2225.
101. Herzfeld, J.; Berger, A.E. Sideband intensities in NMR spectra of samples spinning at the magic angle. *J. Chem. Phys.* **1980**, *73*, 6021–6030, https://doi.org/10.1063/1.440136.
102. Fernandez-San Millan, A.; Fernandez-Irigoyen, J.; Santamaria, E.; Larraya, L.; Farran, I.; Veramendi, J. *Metschnikowia pulcherrima* as an efficient biocontrol agent of Botrytis cinerea infection in apples: Unraveling protection mechanisms through yeast proteomics. *Biol. Control.* **2023**, *183*, 105266, https://doi.org/10.1016/j.biocontrol.2023.105266.
103. Błaszczyk, U.; Wyrzykowska, S.; Gąstoł, M. Application of Bioactive Coatings with Killer Yeasts to Control Post-Harvest Apple Decay Caused by *Botrytis cinerea* and *Penicillium italicum*. *Foods* **2022**, *11*, 1868, https://doi.org/10.3390/foods11131868.
104. Sepúlveda, X.; Vargas, M.; Vero, S.; Zapata, N. Indigenous Yeasts for the Biocontrol of *Botrytis cinerea* on Table Grapes in Chile. *J. Fungi* **2023**, *9*, 557., https://doi.org/10.3390/jof9050557.
105. Zajc, J.; Černoša, A.; Sun, X.; Fang, C.; Gunde-Cimerman, N.; Song, Z.; Gostinčar, C. From Glaciers to Refrigerators: the Population Genomics and Biocontrol Potential of the Black Yeast *Aureobasidium subglaciale*. *Microbiol. Spectr.* **2022**, *10*, e01455-01422, https://doi.org/10.1128/spectrum.01455-22.
106. González-Gutiérrez, K.N.; Ragazzo-Sánchez, J.A.; Barros-Castillo, J.C.; Narváez-Zapata, J.A.; Calderón-Santoyo, M. Yeasts with potential biocontrol of Colletotrichum gloeosporioides in avocado (Persea americana Mill. cv. Hass) and characterization of Yamadazyma mexicana mechanisms. *Eur. J. Plant Pathol.* **2023**, *165*, 525-543, https://doi.org/10.1007/s10658-022-02625-4.
107. Chen, O.; Hong, Y.; Ma, J.; Deng, L.; Yi, L.; Zeng, K. Screening lactic acid bacteria from pickle and cured meat as biocontrol agents of Penicillium digitatum on citrus fruit. *Biol. Control* **2021**, *158*, 104606, https://doi.org/10.1016/j.biocontrol.2021.104606.
108. Bhan, C.; Asrey, R.; Singh, D.; Meena, N.K.; Vinod, B.R.; Menaka, M. Bioefficacy of bacteria and yeast bioagents on disease suppression and quality retention of stored *Kinnow mandarin* fruits. *Food Biosci.* **2023**, *53*, 102743, https://doi.org/10.1016/j.fbio.2023.102743.
109. Delali, K.I.; Chen, O.; Wang, W.; Yi, L.; Deng, L.; Zeng, K. Evaluation of yeast isolates from kimchi with antagonistic activity against green mold in citrus and elucidating the action mechanisms of three yeast: *P. kudriavzevii*, *K. marxianus*, and *Y. lipolytica*. *Postharvest Biol. Technol.* **2021**, *176*, 111495, https://doi.org/10.1016/j.postharvbio.2021.111495.

110. Abd-El-Khair, H.; Elshahawy, I.E.; Haggag, H.E.K. Field application of Trichoderma spp. combined with thiophanate-methyl for controlling Fusarium solani and Fusarium oxysporum in dry bean. *Bull. Natl. Res. Cent.* **2019**, *43*, 19, https://doi.org/10.1186/s42269-019-0062-5.
111. Zhou, Q.; Fu, M.; Xu, M.; Chen, X.; Qiu, J.; Wang, F.; Yan, R.; Wang, J.; Zhao, S.; Xin, X.; Chen, L. Application of antagonist *Bacillus amyloliquefaciens* NCPSJ7 against *Botrytis cinerea* in postharvest Red Globe grapes. *Food Sci. Nutr.* **2020**, *8*, 1499-1508, https://doi.org/10.1002/fsn3.1434.
112. Wang, X.-L.; Qiu, S.-Y.; Zhou, S.-Q.; Xu, Z.-H.; Liu, X.-T. Phosphate-Solubilizing Capacity of *Paecilomyces lilacinus* PSF7 and Optimization Using Response Surface Methodology. *Microorganisms* **2023**, *11*, 454, https://doi.org/10.3390/microorganisms11020454.
113. Arif, S.; Farooq Hussain Munis, M.; Liaquat, F.; Gulzar, S.; Haroon, U.; Zhao, L.; Zhang, Y. *Trichoderma viride* establishes biodefense against clubroot (*Plasmodiophora brassicae*) and fosters plant growth via colonizing root hairs in pak choi (*Brassica campestris* spp. *chinesnsis*). *Biol. Control* **2023**, *183*, 105265, https://doi.org/10.1016/j.biocontrol.2023.105265.
114. Sandy, Y. A.; Chen, Y.-C.; Sulistyowati, L. Purification and Identification of an Antifungal Protein from an Isolated Fungus with Antagonism to Colletotrichum gloeosporioides MC9. *AGRIVITA J. Agric. Sci.* **2022**, *44*, 332–343, https://doi.org/10.17503/agrivita.v44i2.2966.
115. Hammami, R.; Oueslati, M.; Smiri, M.; Nefzi, S.; Ruissi, M.; Comitini, F.; Romanazzi, G.; Cacciola, S.O.; Sadfi Zouaoui, N. Epiphytic Yeasts and Bacteria as Candidate Biocontrol Agents of Green and Blue Molds of Citrus Fruits. *J. Fungi* **2022**, *8*, 818, https://doi.org/10.3390/jof8080818.
116. Li, S.; Xu, X.; Zhao, T.; Ma, J.; Zhao, L.; Song, Q.; Sun, W. Screening of *Bacillus velezensis* E2 and the Inhibitory Effect of Its Antifungal Substances on *Aspergillus flavus*. *Foods* **2022**, *11*, 140, https://doi.org/10.3390/foods11020140.
117. Ruangwong, O.-U.; Pornsuriya, C.; Pitija, K.; Sunpapao, A. Biocontrol Mechanisms of *Trichoderma koningiopsis* PSU3-2 against Postharvest Anthracnose of Chili Pepper. *J. Fungi* **2021**, *7*, 276, https://doi.org/10.3390/jof7040276.
118. Ntemafack, A.; Chouhan, R.; Kapoor, N.; Kumar, A.; Dhiman, S.K.; Manhas, R.S.; Chaubey, A.; Hassan, Q.P.; Gandhi, S.G. Protective effect of *Bacillus* species associated with *Rumex dentatus* against postharvest soil borne disease in potato tubers and GC–MS metabolite profile. *Arch. Microbiol.* **2022**, *204*, 583, https://doi.org/10.1007/s00203-022-03213-0.
119. Podgórska-Kryszczuk, I. Biological Control of *Aspergillus flavus* by the Yeast *Aureobasidium pullulans* In Vitro and on Tomato Fruit. *Plants* **2023**, *12*, 236, https://doi.org/10.3390/plants12020236.
120. Chen, C.; Cao, Z.; Li, J.; Tao, C.; Feng, Y.; Han, Y. A novel endophytic strain of *Lactobacillus plantarum* CM-3 with antagonistic activity against *Botrytis cinerea* on strawberry fruit. *Biol. Control* **2020**, *148*, 104306, https://doi.org/10.1016/j.biocontrol.2020.104306.
121. Agarbati, A.; Canonico, L.; Pecci, T.; Romanazzi, G.; Ciani, M.; Comitini, F. Biocontrol of Non-*Saccharomyces* Yeasts in Vineyard against the Gray Mold Disease Agent *Botrytis cinerea*. *Microorganisms* **2022**, *10*, 200, https://doi.org/10.3390/microorganisms10020200.

Publisher's Note & Disclaimer